Epidermal stratification is uncoupled from centrosome-dependent cell division orientation of the basal progenitors

Mareike Damen[1,2], Ekaterina Soroka[1,2], Houda Khatif[1,2], Christian Kukat[3], Benjamin D. Simons[4], Hisham Bazzi[1,2,*]

[1]Department of Dermatology and Venereology, University Hospital of Cologne, University of Cologne, 50931 Cologne, Germany

[2]The Cologne Cluster of Excellence in Cellular Stress Responses in Aging-associated Diseases (CECAD), University of Cologne, 50931 Cologne, Germany

[3]FACS and Imaging Core Facility, Max Planck Institute for Biology of Aging Research, 50931 Cologne, Germany

[4]The Welcome Trust/Cancer Research UK Gurdon Institute, University of Cambridge, Cambridge CB2 1QN, UK

*Correspondence: hisham.bazzi@uk-koeln.de (H.B.)

Key words: delamination, centriole, cilia, p53, 53BP1, USP28

Abstract

The development of complex stratified epithelial barriers in mammals is initiated from single-layered epithelia. How stratification is initiated and fueled are still open questions. Previous studies on skin epidermal stratification suggested a central role for perpendicular/asymmetric cell division orientations of the basal keratinocyte progenitors. Here, we use centrosomes, that organize the mitotic spindle, to test whether cell division orientations and stratification are linked. Genetically ablating centrosomes from the developing epidermis led to the activation of the p53-, 53BP1- and USP28-dependent mitotic surveillance pathway causing a thinner epidermis and hair follicle arrest. Importantly, the centrosome/p53 double mutant keratinocyte progenitors significantly altered their division orientations without affecting epidermal stratification. Time-lapse imaging and tissue growth dynamic measurements suggested that early stratification is initiated by a burst in basal and suprabasal cell proliferation as well as cell delamination. The data provide insights for tissue homeostasis and hyperproliferative diseases that may recapitulate developmental programs.

Introduction

The generation of complex stratified epithelia, including the skin epidermis, during mammalian embryonic development is essential to form barriers that are compatible with postnatal life [1]. The stratified skin epidermis is initiated from the single-layered simple epithelium, derived from the ectoderm, surrounding the embryo [2]. Around embryonic day (E) 9.5, the epithelial cells commit to stratification through the master regulator p63, a member of the p53 family of transcription factors [3,4]. The progenitor cells down-regulate the expression of the simple-epithelial keratin intermediate filaments, such as Keratin-8 (K8), and express the complex-epithelial keratins, K5 and K14. The periderm is the first layer generated and it acts as a transient protective and insulating barrier for the developing embryo [5]. Around E12.5, the first differentiated suprabasal epidermal layer cells appear and are characterized by the expression of a distinct set of keratins, K1 and K10 [6]. Subsequently, the epidermal keratinocytes undergo further differentiation and crosslinking to generate a fully functional barrier by E17.5 [7]. The stereotypical regeneration and differentiation program in the epidermis, starting from the basal stem cells, persists throughout the life of the animal to replenish the shed corneocytes [8]. In addition to the interfollicular epidermal stem cells, the basal keratinocyte progenitors also give rise to all the stem cells of the skin epithelium including the hair follicle stem cells [9].

The mechanism of how the new layers of the stratified epidermis are generated is still not well-understood. The published data support a model for interfollicular epidermal stratification that is coupled to the orientation of cell division in the basal layer of the epidermis [2,10]. At E12.5 and earlier, almost all of the progenitor basal cells divide with an axis that is parallel to the basement membrane and undergo a presumptive symmetric division to generate two progenitor daughter cells that remain in the basal layer [11]. From E13.5 onwards, more of the dividing basal progenitors shift their axis of division to a perpendicular orientation, which is now synonymous with an asymmetric division, to generate one daughter progenitor cell that remains in the basal

layer, and one differentiated daughter cell that stratifies the forming epidermis [11,12]. Several studies in the literature are consistent and correlate with the division orientation-based model [10,13-15]. For example, manipulations in gene products that result in a thinner epidermis, such as knockdown of LGN or NuMa1, are highly associated with an increase in the fraction of parallel divisions, whereas those causing a thickened hyperdifferentiated epidermis, such as overexpression of INSC, are correlated with an increase in the fraction of perpendicular divisions [12]. In this study, we use centrosome loss of function to define the causal relationship between progenitor division orientation and epidermal stratification.

Centrosomes are major microtubule-organizing centers of animal cells that are composed of a pair of centrioles surrounded by a proteinaceous matrix [16]. Centrosomes are essential to provide the centriolar template for cilia, and are important for efficient mitotic spindle assembly [17]. In humans, mutations in genes encoding centrosomal proteins lead to primordial dwarfism and microcephaly [18]. We have previously shown that the constitutive ablation of *Sas-4*, a gene essential for centriole formation and duplication, led to the loss of centrioles and cilia in early developing mouse embryos [19]. The loss of centrioles, but not the secondary loss of cilia, resulted in p53-dependent cell death and embryonic arrest at E9.5 [19]. Conditional ablation of *Sas-4* in the developing brain recapitulated the human microcephaly phenotype and led to p53-dependent cell death of the radial glial progenitors (RGPs) in the cortex [20]. Activation of this p53-dependent pathway was independent of DNA damage or chromosome segregation errors, and instead was associated with prolonged mitotic duration [19,20]. Recent reports in cultured mammalian cell lines have confirmed our findings and extended them to include 53BP1 and USP28 as new components acting upstream of p53 in a novel pathway now termed “the mitotic surveillance pathway” [21-26].

Published data on brain development suggested that neurogenesis in the brain cortex depends on the regulation of cell division orientation of the RGPs in the ventricular zone of the cortex [27]. However, the *Sas-4*; *p53* double mutant RGPs showed randomized cell division orientation relative to controls, yet resulted in proper cortical development and layering [20]. In this work, we conditionally removed *Sas-4* and centrioles from the developing skin epidermis to test whether the keratinocyte basal progenitors can uncouple cell division orientation from epidermal stratification and differentiation. To separate the functions of centrioles in cilia formation versus spindle assembly, we also conditionally removed *Ift88*, a gene required for the formation of cilia but not centrioles [28-30]. Our data showed that the loss of centrioles, but not cilia, resulted in early p53-dependent cell death, leading to a thinner epidermis and arrested hair follicles. These phenotypes were rescued in the *Sas-4*; *p53* double mutant epidermis, which resembled controls and cilia mutants. Importantly, the double mutant basal keratinocyte progenitors showed a significant shift in cell division orientation that was uncoupled from proper epidermal stratification and differentiation. Using time-lapse imaging in skin explants and measurements of tissue growth dynamics in developing embryos, the data supported a revised model of epidermal stratification that is based on cell delamination and a burst in proliferation in basal and suprabasal progenitors.

Results

Centrioles are important for proper mouse epidermal and hair follicle development

In order to assess the functions of mammalian centrioles and centrosomes in the developing mouse skin epithelium, we deleted *Sas-4* using a *K14-Cre* line [31], which expresses the Cre recombinase in developing stratified epithelia, including the skin epidermis as early as embryonic day (E) 9.5, in combination with a *Sas-4* conditional allele [19,20]. Immunostaining for γ-Tubulin (TUBG, a marker for centrosomes) and CEP164 (a marker for centriolar distal appendages) confirmed that centrioles are almost completely lost from the epidermal basal and suprabasal cells by E15.5 (Fig. S1A, B). At postnatal day 21 (P21), the centrosome mutant mice were smaller than their control littermates and had a grossly thin and transparent skin with very sparse hair (Fig. 1A, Fig. S1C). Starting as early as P4, the centrosome mutant mice were significantly smaller than their littermates (Fig. S1C), likely due to the *K14-Cre; Sas-4* defects in the oral epithelium which impaired food intake. To avoid any secondary complications of centriole loss after birth, we focused most of our analyses on embryonic development until P0.

At P0, the *Sas-4* mutant epidermis was significantly thinner than that of control littermates with a marked reduction in the number of hair follicles (Fig. 1A-C). To study if the epidermal differentiation process was affected upon the loss of centrioles, we performed immunostainings on newborn back-skin sections. Staining for markers of the proliferative basal layer (K14), and differentiated layers (K1 and Loricrin, LOR), showed that although the epidermis as a whole was thinner, the differentiation process was not majorly affected in the *Sas-4*/centrosome mutant epidermis (Fig. 1D). However, the upregulation of K6A indicated an abnormal response in the *Sas-4* mutant skin epithelium (Fig. 1D). Consistent with the reduced viability of the centrosome mutant animals by P3 (~60% compared to ~95 % for control animals), the embryos at E17.5 showed a slight delay in skin barrier formation at the chin and the paws, as judged by a Toluidine Blue dye-penetration assay, which was restored just before birth at E18.5 (Fig. S1D).

To test whether the secondary loss of cilia upon the removal of centrioles caused the centrosome-mutant phenotypes, we used the *K14-Cre* line and a conditional allele of *Ift88* [28-30]. Immunostaining for TUBG and ARL13B (a marker for cilia) showed the presence of centrosomes but the loss of cilia in the *Ift88* mutant epidermis at E15.5 (Fig. S1E, F). Compared to *Sas-4*/centrosome mutants, we did not observe major skin phenotypes in the epidermis and hair follicles of *Ift88*/cilia mutants, as judged by morphological, histological and immunofluorescence examination (Fig. 1, Fig. S1G), indicating that the centrosome mutant phenotypes are not due to the loss of cilia.

We concluded that, in contrast to cilia, centrioles and centrosomes are important to ensure normal development of the skin epithelium; however, despite the centriole deficiency in the basal keratinocyte progenitors, they showed robust regulation to allow the formation and maintenance of a generally functional skin barrier.

The loss of centrioles in the epidermis activates the mitotic surveillance pathway

Next, we used immunostaining to assess the molecular consequences of the loss of centrioles in the epidermis. The data showed that there was an upregulation of p53 and cell death, marked by Cleaved-Caspase 3 (Cl.CASP3) (Fig. 2A-C). In contrast, no upregulation of p53 was observed in the *Ift88*/cilia mutant epidermis at E15.5 (Fig. S2A), indicating that cilia loss alone did not activate the same pathway [19,20]. In the newborn epidermis, cell death was rarely detected while p53 was still high in the basal keratinocytes of centrosome mutants compared to controls (Fig. S2B-D). To check whether the high p53 in the centrosome mutant keratinocytes at P0 caused cell cycle arrest in G1 instead of cell death, similar to the reports in mammalian cell lines that lose centrioles *in vitro* (Fig. 2D) [21,22,32], we performed cell cycle analyses on isolated epidermal

keratinocytes of newborn mice. The cell cycle profiles showed no significant increase in the G1 population in centrosome mutant keratinocytes compared to controls (Fig. S2E).

Centriole loss causes prolonged mitotic duration which increases the mitotic index [19]. We quantified the number of mitotic cells, marked by phospho-Histone H3 (pHH3), in the basal layer of the epidermis of centrosome mutants and controls at E15.5 (Fig. S2F). We observed an increase in the mitotic index in the centrosome mutant epidermis compared to the control littermates (Fig. S2F) [19,20]. The delay in mitosis in centrosome mutants was also reflected in a slight, but not significant, increase in the G2/M keratinocyte population at P0 (Fig. S2E), likely because mitosis constitutes only a minor fraction of the total cell cycle (~3-4 %). Centrioles are required for efficient mitosis, which is associated with the suppression of the activation of the p53-dependent mitotic surveillance pathway (Fig. 2D) [26]. We tested whether the loss of p53 can bypass the activation of this pathway in the centrosome mutant skin epidermis (Fig. 2E). We observed that the simultaneous knockout of *p53* in the *Sas-4*/centrosome mutant skin epidermis significantly rescued the gross epidermal and hair follicle defects, including the epidermal thickness and hair follicle numbers (Fig. 2E-G). However, the loss of p53 does not rescue cilia formation or prolonged mitosis, because it does not restore centrioles [19], and the double mutants still showed a higher mitotic index compared to controls (Fig. S2F).

We then asked whether the loss of *Usp28* or *53bp1,* which have been implicated in the activation of the mitotic surveillance pathway in human cell lines *in vitro* (Fig. 2D) [23-25]*,* would recapitulate the p53 deficiency in centrosome mutants *in vivo.* We generated *Usp28* and *53bp1* mutant mice using CRISPR/Cas9 (see Methods) and crossed each allele to the *Sas-4* conditional mutants and *K14-Cre* to generate *Sas-4; Usp28* and *Sas-4; 53bp1* double mutant skin epidermis. Remarkably, our data showed that these mice had a phenotypic rescue similar to the *Sas-4; p53* double mutants, establishing their essential role in the p53-dependent pathway *in*

vivo (Fig. 2E-G). These rescues were quite significant even though our CRISPR/Cas9-generated mutations in *Usp28* and *53bp1* had residual proteins by immunostaining (Fig. S2G, H), suggesting that they are likely to be hypomorphic alleles.

The orientation of cell division in the basal progenitors does not correlate with cell fate in the centrosome mutant epidermis

The centrosome/p53 double mutant, which showed normal epidermal thickness at birth (Fig. 2E, G), allowed us to examine the consequences of the loss of centrioles in regulating cell division orientation and its relationship to epidermal stratification. We used immunostaining for Integrin-α6 (ITGA6), to mark the basement membrane zone, and Survivin, a mid-body marker to highlight the mitotic cells in late anaphase to telophase when division orientation is final, and measured the angles of cell division orientations in sections of the back-skin of *Sas-4; p53* double mutant and control animals (Fig. 3A) [12]. Published reports consider E16.5 and E17.5 as the peak of epidermal stratification, with a fine balance between parallel (0-29°) and perpendicular (60-90°) division orientations [33]. To our surprise, the measurements showed a significant shift towards more perpendicular cell division orientations in the *Sas-4; p53* double mutant skin epidermis (~60 %) at both E16.5 and E17.5 compared to wild-type and *p53* mutant controls (~40 %) (Fig. 3B, C; Fig. S3A, B). The increase in perpendicular division orientations in the mutants was accompanied by a significant decrease in parallel division orientation at both timepoints (~15-20 % in the mutants compared to ~40 % or more in controls) (Fig. 3B, C; Fig. S3A, B). The shift from parallel to perpendicular division orientation in the mutants was still significant even after the oblique division orientations (30-59°) were distributed in a new parallel (0-44°) and perpendicular (45-90°) bins (Fig. S3C).

We next tested if our data were consistent with the current model of basal keratinocyte progenitors' division orientation determining the balance between proliferation and

differentiation. First, if perpendicular division orientations were asymmetric in nature, then an increase in their proportion should lead to more differentiation in the mutants. Thus, we measured the thickness of the K1-positive suprabasal layers at E16.5, and the data showed that it was not changed in the mutants relative to controls (Fig. 3D, E). In addition, the skin epidermal histology and thickness in the *Sas-4; p53* double mutant skin at birth were also similar to controls (Fig. 2E-G). Second, if parallel division orientations were symmetric, then a decrease in their proportion should result in a lower density of basal keratinocyte progenitors. Instead, the *Sas-4; p53* double mutant skin epidermis showed an increase in the density of basal cells compared to controls (Fig. 3F), a phenotype that seemed to be dependent on p53 and/or cilia (Fig. S3D). We then checked whether increased proliferation could explain the maintenance, or even increase, in the number of basal cells in the mutants, but the data using EdU incorporation showed no difference between mutants and controls (Fig. S3E). In this context, our data suggested that basal keratinocyte progenitors' proliferation and differentiation were uncoupled from cell division orientation during epidermal skin development.

Asymmetric cell division may not be essential for skin epidermal stratification during development

Because our data suggested that basal progenitor division orientation may not necessarily dictate epidermal stratification and differentiation, we next asked whether cell division *per se* was essential for the formation of a stratified epidermis. Embryonic development on the organismal level is reliant on proliferation and cell division *in vivo*. Therefore, we used a well-established *ex vivo* developing mouse skin culture which recapitulates epidermal differentiation as well as hair follicle development [34] (Fig. 4). We treated skin explant cultures at E13.5, which had only a thin K10-positive differentiated layer, briefly with Mitomycin C (MMC) to stop proliferation and cell division, and then incubated the explants for one (E14.5) or two (E15.5) days [35]. Proliferation and cell division were completely inhibited in the MMC-treated skin explants compared to

controls, as assayed by EdU incorporation and pHH3 staining at E14.5 and E15.5 (Fig. 4A). Importantly, despite the inhibition cell division, the MMC-treated skin epidermis retained the capacity to stratify and differentiate, as shown by the substantial increase in the K10-positive layer thickness at E14.5 and E15.5 (Fig. 4B). Moreover, the number of basal K10-negative cells sharply decreased in the MMC-treated explants compared to the corresponding controls at E14.5 and E15.5 (Fig. 4C). In addition, the number of K10-expressing suprabasal cells in the MMC-treated explants increased ~4-fold at E14.5 and E15.5 compared to the E13.5 controls, but was still significantly lower than that in the vehicle-treated controls (Fig. 4D). The cell number deficiency in the MMC-treated skin cultures was not unexpected because of the inhibition of proliferation and elevated cell death (Fig. S4). The data suggested that cellular proliferation and cell division are not absolutely essential for skin epidermal stratification and differentiation, indicating that other mechanisms, such as cell delamination, can contribute to these processes, in particular, when cell division is inhibited.

Time-lapse imaging reveals an epidermal basal layer flexibility and cellular delamination

We then asked whether perpendicular cell division orientations and/or cellular delamination of the basal progenitors contribute to epidermal stratification and the formation of the suprabasal layers. We recorded time-lapse movies of the skin explants on filters between E13.5-E15.5 [36]; however, the Z-dimension resolution was not sufficient to follow dividing cells (Fig. S5A). Thus, we flipped the explants to transform the initial Z-dimension into an XY-plane (see Methods). The new culture method did not affect skin epidermal stratification and differentiation as shown by K10 staining, and even better resembled the embryonic skin *in vivo* than the flat skin cultures (compare Fig. S5B and C). We focused on the daughter cells of perpendicularly dividing basal progenitors (~80-90°) that point away from the epidermal-dermal interface, and assessed their position over time. Our data showed that almost half of these cells can be incorporated close to the neighboring basal cells (Fig. 5A, Movie S1), whereas the other half remained in the second

layer (Fig. 5B, Movie S2). Moreover, we observed progenitor basal cells that delaminated, moved up and eventually divided suprabasally (Fig. 5C, Movie S3). The data from the time-lapse experiments suggested that the progenitors in the basal layer stratify by delamination and suprabasal divisions to form the multi-layered epidermis, independent of cell division orientation.

During our analyses of the developing mouse embryonic skin epidermis, we noticed that the basal layer character does not necessarily require that the basal keratinocytes are in direct contact with the underlying basement membrane. This was particularly evident upon staining with ITGA6 (basal) and K10/K1 (suprabasal) at different epidermal developmental stages (Fig. 5D). From E13.5-E17.5, ITGA6 was surrounding the entire basal keratinocytes, including some that seemed to be in the second layer but were negative for K10 (Fig. 5D), as well as the daughter cells in a perpendicular division that point away from the epidermal-dermal interface (Fig. 3A). The *ex vivo* skin explant culture on filters at E13.5, which was just released from the stretching tension of the embryo, showed an even thicker (~3 cell layers) ITGA6-positive and K10-negative pseudo-stratified basal layer (Fig. S5C), supporting the *in vivo* data. Collectively, our data suggested that the skin epidermal basal layer is more flexible during development where cells move to a seemingly-second layer, for example during a perpendicular division, but still retain a basal keratinocyte progenitor character.

The developing epidermis stratifies and differentiates in two phases

To gain insight into the data, we turned to a modelling-based approach (*Supplementary Theory* in Methods) informed by measurements of dynamic tissue growth parameters during back-skin interfollicular epidermal development (E12.5-E18.5), in the antero-posterior axis (sagittal sections, Fig. 6) and the dorso-ventral axis (transverse sections, Fig. S6). We quantified the following parameters: 1) the net rate of embryonic growth (Fig. 6A-D), 2) the density of basal and suprabasal cells (Fig. 6E, F; Fig. S6A, B), 3) the proliferation index of basal and suprabasal cells

(Fig. 6G-J; Fig. S6C). Based on our data above (Fig. 5D), we defined basal progenitor cells by their expression of ITGA6 but not K10, whereas suprabasal cells express K10 but not ITGA6. While the total embryonic growth was approximately linear along the different axes between E12.5-E18.5 (Fig. 6B-D), we made two important observations regarding the suprabasal layer. First, the major increase in the number of suprabasal cells occurred between E13.5-E15.5 (Fig. 6E, F; Fig. S6A, B). Second, the suprabasal cells were highly proliferative during the same window of epidermal development (Fig. 6G-J; Fig. S6C), consistent with the data from the time-lapse imaging of skin roll explants (Fig. 5C, Movie S3) [10,37]. Overall, our measurements and modelling support a two-phase behavior for basal and suprabasal cells during epidermal stratification and differentiation. The first phase between E12.5-E15.5 is characterized by proliferation and amplification to fuel stratification, where the suprabasal cells act as a transit-amplifying population that proliferates to populate the newly-forming suprabasal layers. Consistently, the total number of cells rises exponentially by a factor of 7.4 during this phase (Fig. 6K), almost twice the net area expansion of the tissue. In addition, the density of suprabasal cells reaches parity and equilibrium with that of the basal progenitor cells at the end of this phase (at E15.5, Fig. 6F; Fig. S6B). The second phase between E15.5-E18.5 is characterized by a precipitous slow-down in the proliferation rate, especially in the suprabasal cells which largely undergo terminal differentiation (Fig. 6G, H; Fig. S6C). The total number of cells in this second phase rises linearly by a mere factor of 2 (Fig. 6K), in proportion to the net expansion of the tissue. The cell densities in both layers remain similar and largely unchanged during this phase (Fig. 6F; Fig. S6B). Collectively, our data suggest that the major phase of epidermal stratification takes place between E13.5-E15.5 and is boosted by the proliferating new suprabasal cells [10,37].

Discussion

How simple epithelia transform into complex stratified barriers, and whether the initiation of this stratification program is dependent on a shift to perpendicular division orientations of the progenitors, are still open questions in epithelial biology. Here, we use centrosome mutants to disrupt cell division orientation and test its relationship with skin epidermal stratification.

In the *Sas-4* mutant epidermis, the basal keratinocyte progenitors that lost centrioles upregulated p53 and only a small fraction of cells died (~5% with Cl.CASP3) (Fig. 2A-C). In newborns, the basal acentriolar keratinocytes also showed high levels of p53, but only rare cells died (Fig. S2A-C). In contrast, centriole loss in the early embryo and developing brain led to widespread cell death and tissue degeneration (Bazzi and Anderson, 2014; Insolera, 2014). The data indicate that the skin epidermal keratinocytes are more robust than early embryonic and developing brain cells, suggesting that basal keratinocytes adapt to centriole loss to maintain a relatively intact skin barrier. Our findings are consistent with the human skin phenotypes not being prominent features in patients with mutations in genes encoding centrosomal proteins [18]. The Café au Lait skin pigmentation defect is a rarely reported skin phenotype in these patients [38,39]. These skin pigmentation defects are likely due to high p53 and the tanning effect [40].

The skin epithelial centrosome mutants had a thin epidermis and sparse hair (Fig. 1A-C). These two prominent centrosome-associated phenotypes were dependent on the activation of the mitotic surveillance pathway because they were rescued upon the removal of p53, 53BP1 or USP28 (Fig. 2D-G). Given that p63 is the master transcription factor governing epidermal stratification and skin appendage development [4], and that p53 and p63 share a consensus DNA binding site, it is likely that the abnormal increase in p53 levels in the developing skin epithelium of centrosome mutants disrupts p63 functions leading to the skin defects. In addition, to our knowledge, the rescue of the activation of the mitotic surveillance pathway using *53bp1* or

Usp28 mutations in centrosome mutant tissues in mice has not been previously reported. Our data establish the conservation of this pathway in mammalian tissues *in vivo*.

Many signaling pathways have been associated with centrosomes and their extensions, the primary cilia [41]. The phenotypes of the skin epithelial centrosome double mutants (Fig. 2), which also lack cilia, and *Ift88*/cilia mutants (Fig. 1), confirm earlier reports about the requirement of cilia and cilia-associated signaling mainly in postnatal hair follicles during homeostasis [29]. Our genetic data do not support a major link between centrosomes or cilia and Notch signaling in the skin epithelium [30], where Notch signaling plays roles in epidermal and hair shaft differentiation [6,37,42].

Our data show that the daughter cells that point away from the epidermal-dermal interface in a perpendicular division orientation of the basal progenitors are still surrounded by a basement membrane receptor, ITGA6, (Fig. 3A) [43], and can be incorporated in the basal layer following division (Fig. 5A, Movie S1). In addition, in *Sas-4; p53* double mutants, the decrease in the fraction of parallel division orientations and the increase in the perpendicular one in basal keratinocyte progenitors do not lead to a corresponding decrease in basal layer density or hyperdifferentiation (Fig. 3D-F), as predicted by the model that cell division orientation and epidermal stratification are coupled [44]. Our data suggest that a perpendicular division of the basal progenitors in the developing skin epidermis does not necessarily result in an asymmetric cell fate. Moreover, the inhibition of cellular proliferation in the developing skin does not completely abolish cellular differentiation and stratification (Fig. 4). It has been known for a few decades that switching primary mouse skin epidermal keratinocytes in culture to high calcium levels induces differentiation independent of cell division [45]. Based on these findings, we propose that the differentiation of the basal layer keratinocytes in the developing epidermis maybe the default pathway and a basal-layer character is actively maintained by continuously

remaining in the cell cycle (MMC-experiment in skin explants, Fig. 4). The data suggest that commitment to differentiation in the basal progenitors is a multi-step process that is independent of division orientation (Fig.s 3; Fig. 5A, B; Movies S1-S2), and is associated with cellular detachment or delamination (Fig. 5C, Movie S3), similar to earlier reports in the developing skin as well as in the adult mouse skin epidermis [46,47]. It is worth noting that perpendicular divisions have only been rarely observed in the adult skin epidermis [46,48].

It has recently been shown that cellular geometry of the epidermal basal progenitors correlate with cell division orientation in different body sites in the developing embryo at E14.5 [49]. However, all the skin body sites generate a stratified epidermis and a fully functional barrier by E17.5 (Fig. S1D) [7]. Our data support a model whereby a thin back-skin epidermis at E12.5 mechanically favors parallel division orientations in basal keratinocytes. As development proceeds and more suprabasal layers are added, the thickened epidermis allows perpendicular cell division orientations in the basal layer. Then, in adult life the skin epidermis is thin again and predominantly ensures parallel division orientations of basal keratinocytes. In our opinion, the correlations between a thinner epidermis and parallel division orientations, or between a thicker epidermis and perpendicular division orientations of the progenitors, can be explained by the topology of the epidermis restraining the cell division orientation, rather than the prevailing opposite causal relationship [10,50].

Collectively, our data support a two-phase model of physiological epidermal stratification, the first phase between E12.5-E15.5 is mainly fueled by the higher proliferation rates of the basal cells and the newly-produced K10-positive, transit-amplifying and suprabasally-committed cells (Fig. 7)[37]; whereas the second phase between E15.5-E18.5 is a maintenance phase which is perhaps supported by cellular delamination from the basal layer, and is contiguous with postnatal epidermal growth and turnover (Fig. 7). It is intriguing to speculate whether the adult

mouse or human epidermis recapitulates these phases during normal homeostasis, or in certain disease conditions that are characterized by hyperproliferation or hyperdifferentiation. Why and how certain basal progenitor cells commit to delamination and differentiation in both phases are still open questions. For the first phase, cellular crowding and chance extrusion maybe the dominant forces [47]. Perhaps the choice to delaminate is stochastic in nature, as has been shown for the adult skin epidermis and even other epithelia [46,48]. In this respect, a weak noisy signal, such as Notch signaling, is amplified and fixed by the cells committed to delaminate and differentiate, while concomitantly inhibiting the surrounding cells from adopting the same fate [6,37,51,52].

Acknowledgement

We thank our colleagues at the University of Cologne and SFB829: Carien Niessen, Sara Wickström (University of Helsinki, Finland), Sandra Iden, Catherin Niemann, Mirka Uhlirova, Leo Kurian and Lisa Wirtz for critical discussions about the work and comments on the manuscript. We thank Terry Lechler (Duke University, USA) and Scott Williams (University of North Carolina, USA) for valuable suggestions during their sabbaticals in Cologne. We thank David Gonzalez and Valentina Greco (Yale University, USA) for their advice on time-lapse imaging analyses. We acknowledge and appreciate the CECAD *in vivo* research facility (Branko Zevnik) for the generation of the new mouse lines of *53bp1 and Usp28*, and rederivation and maintenance of the other lines. We thank the CECAD imaging facility, especially Peter Zentis for image analyses, and Hans Fried and Christoph Möhl of the DZNE Imaging and Data Analysis Facilities (Bonn, Germany). Special thanks to Hironobu Fujiwara and Ritsuko Morita (RIKEN Center, Japan) for sharing unpublished data on vibrissae pad imaging. The work was funded by the Deutsche Forschungsgemeinschaft (DFG, German Research Fundation)- Project-ID 73111208 - SFB 829 “Molecular Mechanisms regulating Skin Homeostasis”. The project was also supported by the DFG under Germany's Excellence Strategy – CECAD, EXC 2030 – 390661388. The funders had no role in study design, data collection and analysis, decision to publish, or preparation of the manuscript.

Author contributions

Conceptualization: H.B. and M.D.; Methodology: H.B., M.D. and B.D.S.; Software: E.S., M.D. and H.B.; Formal Analysis: M.D, H.B., E.S. and B.D.S.; Investigation: M.D., E.S., H.K. and H.B.; Resources: C.K.; Writing: H.B. and M.D.; Visualization: M.D. and H.B.; Supervision, Project administration and Funding Acquisition: H.B.

Declaration of interests

The authors declare no competing interests.

Methods

Animals and Genotyping

The following mouse alleles were used in this study: *Sas-4*$^{f/f}$ (Cenpj$^{tm1c(EUCOMM)Wtsi/tm1d(EUCOMM)Wtsi}$) [19], *Ift88*$^{f/f}$ (Ift88$^{tm1Bky/tm1.1Bky}$) [28], *K14-Cre* [31], *p53*$^{f/f}$ (Trp53$^{+tm1.Brn/tm1.1Brn}$) [53], H2B-EGFP (CAG::H2B-EGFP) [54]. The CRISPR/Cas9 endonuclease-mediated knockout (em) mouse knockouts of *53bp1*$^{em/em}$ (*Trp53bp1*$^{em/em}$) and *Usp28*$^{em/em}$ were generated by the CECAD *in vivo* Research Facility (ivRF) using microinjection of the corresponding gRNA, Cas9 mRNA and Cas9 protein into fertilized zygotes:

	53bp1	***Usp28***
Exon	Exon 2	Exon 2
gRNA	TACTGGAAGTCAATTGGATT	AATCAGCTGCGAGAAATCAC
Mutation	31 bp deletion	16 bp deletion
Deleted	GGACCCTACTGGAAGTCAATTGGATTCAGAT	CTGCGAGAAATCACAG
Primer 1	TCGAACTGATCTTTTGTTATTCCA	TCAAAAACAGAGCTGCCAGA
Primer 2	GAACAGGGCATCATCACTCA	CACACCTGACATGTGGGAAA

All phenotypes were analyzed in the FVB/NRj background. The littermates that had the Cre-recombinase and were heterozygous for the floxed or knockout alleles were used as preferred controls where available. Genotyping was carried out using published or standard PCR protocols.

The animals were generated, housed and bred under standard conditions in the CECAD ivRF. The generation and breeding described were approved by the Landesamt für Natur, Umwelt, und Verbraucherschutz Nordrhein-Westfalen (LANUV), Germany (animal applications: 84-02.04.2014.A372, 84-02.04.2015.A405 and 81-02.04.2019.A476).

Histological analysis

Skin or embryo samples were fixed overnight in 10 % Formalin or 4 % Paraformaldehyde (PFA), respectively, washed with 1x PBS and stored in 70 % ethanol for several days. After dehydration, the samples were embedded in paraffin and sectioned on an RM2255 microtome (Leica Biosystems) at 8 µm. For histological analyses, the skin sections were stained with hematoxylin and eosin (H&E) and mounted with Entellan® (Merck). The stained slides were imaged using a DM2000 light microscope (Leica biosystems) or scanned with an SCN400 Slide scanner (Leica biosystems) for subsequent analyses.

Immunofluorescence and Imaging

Embryos were fixed in 4 % PFA overnight at 4 °C, washed with 1x PBS and then cryoprotected in 10-30 % sucrose in 1x PBS overnight at 4 °C. After embedding in Tissue-Tek® (Optimal Cutting Temperature Compound (OCT), Sakura Finetek USA INC), the blocks were sectioned on a CM1850 Cryostat (Leica Biosystems) at 7-10 µm. Postnatal skin samples for immunofluorescence staining were fresh-frozen in OCT and sectioned as above.

For immunofluorescence staining, skin sections were fixed for 10 minutes (min) in 4 % PFA and washed with 1x PBS prior to the common staining protocol: skin or embryo sections were fixed in ice-cold methanol for 10 min at -20 °C, washed with washing buffer containing 0.2 % TritonX-100 in 1x PBS and blocked for 1 hour (h) in blocking buffer containing washing buffer and heat-inactivated goat serum (1 % for embryo and 10 % for skin sections). Mouse IgG Fab fragments were used at 1:10 to block background staining when using mouse primary antibodies (cat#115-007-003, Jackson Laboratories). After the primary antibodies were incubated over night at 4 °C, the sections were washed with washing buffer, incubated with the secondary antibody and DAPI for 1 h at RT and mounted with Prolong Gold (Cell Signaling). Images were obtained using an SP8 confocal microscope (Leica microsystems) or a Meta 710 confocal microscope (Zeiss).

Antibodies

The following primary antibodies were used in this study:

Antigen	Source/ Isotype	Company	Catalog number	Working dilution
53BP1	rabbit	Novus Biologicals	NB100-305SS	1:1000
ARL13B	rabbit	Proteintech	17711-1-AP	1:1000
CEP164	rabbit	Proteintech	22227-1-AP	1:2000
Cleaved-Caspase3	rabbit	Cell Signaling	9661	1:400
Integrin-α6	rat IgG2a	R&D Systems	MAB13501	1:1000
Keratin1	rabbit	BioLegend	905601	1:4000
Keratin10	guinea pig	Progen	GP-K10	1:400
Keratin14	guinea pig	Progen	GP-CK14	1:400
Keratin6A	rabbit	BioLegend	905701	1:4000
Loricrin	rabbit	BioLegend	905101	1:2000
p53 (CM5)	rabbit	Linaris	LIN-P956	1:1000
Phospho-Histone H3	rabbit	Merck	06-570	1:400
Survivin	rabbit	Cell Signaling	2808	1:400
USP28	rabbit	Sigma Aldrich	HPA006778	1:500
γ-Tubulin	mouse IgG1	Sigma Aldrich	T6557	1:2000

Secondary antibodies were Alexafluor® 488, 568, or 647 conjugates (Life Technologies, Invitrogen (ThermoFisher)) and used at 1:1000 in combination with DAPI at 1:1000 (AppliChem A4099).

Keratinocyte isolation

Newborn mice were decapitated, transferred through a disinfection series (Betaisodona, 1x PBS

1:1; Octenisept; 1x PBS; 70 % ethanol; 1x PBS; antibiotic/antimycotic solution in 1x PBS 1:100) and skinned. The skins were incubated overnight at 4 °C in a 5 mg/ml dispase II solution in DMEM/Hams-F12 (without supplements). After the epidermis was separated from the dermis, the epidermis was floated with the basal side down on 1 ml of 0.25 % Trypsin (without EDTA, Gibco) for 20 min at room temperature (RT). Then, keratinocyte medium was used to dissociate the keratinocytes from the epidermis [45,55].

Skin barrier assay

E17.5 or E18.5 embryos were sacrificed by making a cut in the neck to sever the spinal cord, and tail tips were taken for genotyping. After incubating the embryos for 2 min each in an increasing and then decreasing methanol series and washing in 1x PBS, they were stained in a 0.1 % toluidine blue solution in water for 1-2 min on ice. A specific dye pattern showing possible barrier defects appeared after de-staining the embryos in 1x PBS on ice [7,56].

Cell cycle analysis

Freshly isolated epidermal keratinocytes were fixed in 70 % ethanol and stored at -20 °C for several weeks. Then they were centrifuged, washed in 1x PBS and resuspended in Propidium Iodide staining solution (10 µg/ml PI, 200 µg/ml RNAse A, 0.1 % TritonX in 1x PBS). After incubating at RT for 30 mins, cell cycle analysis was performed using a LSRFortessa (BD) FACS machine. Data were analyzed using the FlowJo software.

Skin explant culture and EdU assays

Lateral skin explants were taken from E13.5 wild-type embryos and placed on Nucleopore Track-Etch membranes (Whatman) floating on DMEM (Gibco) containing 10 % FBS and 1x antibiotic/antimycotic solution (Gibco) at 37 °C and 5 % CO_2. The explants were treated with either 10 µg/ml Mitomycin C or DMSO (vehicle) in medium for 3 h, washed with 1x PBS and

cultured further in the medium above. Either directly at E13.5, after 1 day (E14.5) or after 2 days (E15.5), 20 µM EdU was added to the media for 2 h, then the explants were washed with 1x PBS and fixed in 4 % PFA for 2 h at RT. After several washes with 1x PBS, the explants were removed from the membrane, cryoprotected in 30 % sucrose overnight at 4 °C and embedded in OCT for immunofluorescence staining (same protocol as for whole embryo sections except using 0.1 % TritonX-100 in PBS). For EdU analyses in embryonic mouse skin, the pregnant females at the corresponding timepoints were injected intra-peritoneally with EdU at 50 mg/Kg and then anesthetized and sacrificed 3h later for embryo collection, fixation and OCT embedding as described above. The skin sections were treated according to the Click-iT^{TM} EdU imaging kit (Thermo Fisher) instructions before performing regular immunofluorescence staining.

Time-lapse Imaging

Lateral skin explants were taken from E13.5 embryos (H2B-EGFP$^{tg/wt}$) and transferred to media (advanced DMEM + 2 mM L-Glutamine + 0.1 mg/ml Penicillin/Streptomycin + 10% FBS) at 37 °C where they formed rolls. The rolls were embedded in 1 % low-melting agarose in media at 37 °C, where the cutting edge was touching the membrane-bottom of a Lumox® dish (Sarstedt). The set agarose was covered with medium and incubated at 37 °C and 5 % CO_2 until imaging. Time-lapse imaging was carried out between E13.5 and E14.5 using an inverted SP8 confocal microscope (Leica microsystems), an inverted Dragonfly Spinning disc confocal microscope (Andor) or an inverted LSM710NLO Two-Photon microscope (Zeiss) with 20x air objectives and incubation at 37 °C and 5 % CO_2.

Image analyses

Epidermal thickness and number of hair follicles were quantified by scanning the histological sections with the SCN400 slide scanner (Leica Biosystems) and analyzing the images using the

Digital Image Hub (Leica Biosystems). The percentage of p53-positive cells in the epidermis was obtained using ImageJ (NIH) and CellProfiler (Broad institute). The clusters of Cl.CASP3-positive cells, the thickness of K1 or K10 layers, the number of basal and suprabasal layer cells, the pHH3-positive cells as well as the centrosome- or cilia-containing cells in the epidermis were analyzed using ImageJ. The angles of basal cell division orientations were obtained from late anaphase or telophase cells in the epidermis by measuring the angle of the division axis (marked by Survivin) with the basement membrane (ITGA6) using ImageJ. The radial histograms were plotted using the OriginPro® software (Origin Lab), while all the other diagrams were generated using Prism (GraphPad). Time-lapse imaging data were manually analyzed using ImageJ (Correct 3D Drift plug-in), Volocity (Improvision) and Imaris (Bitplane).

Statistical Analysis

Two groups or more of data were compared using a two-tailed student's T-test with a cutoff for significance of <0.05, or one-way ANOVA and Tukey's multiple comparisons test, both of which gave similar significance outcomes (Excel or GraphPad Prism). Angle measurements were compared using a two-way ANOVA, Kolmogorov-Smirnov Test and Chi squared Test (GraphPad Prism). The data are presented as the mean ± SD (standard deviation).

Supplementary Theory

In the following, we consider the basis of the "two-phase" model of embryonic epidermal development based on measurements of the net growth of the embryo, the change in the basal and superbasal cell density, and estimates of the cell proliferation rate within the two layers. To determine the overall increase in epidermal basal and suprabasal cell numbers during development, we must combine estimates of the net increase in tissue area (as inferred from the net expansion of the embryo) and cell density. Both are measured with respect to antero-posterior (sagittal) and dorsoventral (transverse, hereafter called orthogonal) axes of the mouse

(Fig. 6A-E; Fig. S6A). Notably, the length of the of the embryo along both axes, $l_{\mathrm{s}}(t)$ and $l_{\mathrm{o}}(t)$, grows approximately linear with time over the entire E12.5-E18.5 time-course (Fig. 6B-D). Alongside this increase, there is also a change in the basal and suprabasal cell density, with the data showing a small differential between the sagittal and orthogonal directions, most likely due to the differential expansion rates along the body axes (Fig. 6E, F; Fig. S6A, B). Therefore, if we define $\rho_{\mathrm{b/s,s/o}}$ as the basal/suprabasal cell density in the sagittal/orthogonal directions, the total basal/suprabasal cell numbers increase in proportion to

$$n_{\mathrm{b/s}}(t) = \rho_{\mathrm{b/s,s}} l_{\mathrm{s}} \times \rho_{\mathrm{b/s,o}} l_{\mathrm{o}}$$

Based on this estimate, over the first three days from E12.5 to E15.5, the total cell numbers (basal and suprabasal) increase approximately exponentially with time, rising by a factor of around 7 (Fig. 6E, F, K; Fig. S6A, B). Notably, this coincides with the time period in which proliferative cells are found in both basal and suprabasal cell layers (Fig. 6G-J; Fig. S6C). After this period, the cell number increase in both basal and suprabasal cell layers is greatly reduced, showing only a factor of 2 increase over the next three days (Fig. 6E, F, K; Fig. S6A, B).

Together, these results suggest a “two-phase” behavior, with an early phase of cell amplification through rounds of cell duplication, followed by a second phase in which basal cells steadily expand to meet the demands of the underlying growing tissue while, at the same time, giving rise to non-cycling suprabasal cells at a rate that allows both layers to expand in an approximately proportionate manner (Fig. 6E, F, K; Fig. S6A, B). Significantly, during the early phase of cell amplification, cells delaminate from the basal layer (potentially by the effects of cell crowding), giving rise to a proliferatively active suprabasal cell layer.

Therefore, to capture quantitatively the first phase of cell amplification, we suppose that the skin epidermis is comprised of equipotent progenitor cells, *p*, that duplicate through division at a constant rate $\lambda = 0.66$ per day.

$$p \xrightarrow{\lambda} p + p$$

Initially (E12.5-E13.5), this increase in cell number is accommodated through the ongoing expansion of the basal cell layer. During the next day (E13.5-E14.5), the basal cell density becomes elevated slightly, while an excess of proliferative cells is transferred – potentially through crowding – to the suprabasal cell layer. This trend continues during the third day of study (E14.5-E15.5), after which the ratio of basal to suprabasal cells reaches roughly parity (Fig. 6E, F, K; Fig. S6A, B). At this time point, the frequency of proliferative suprabasal cells diminishes significantly (Fig. 6G, H; Fig. S6C), suggesting that this last phase is characterized by cell cycle exit consistent with the cells' entry into a terminal differentiation program.

After this point, the data suggest only a modest rate of increase in the number of basal and suprabasal cells, which rise proportionately by a factor of around 2 over the next three days from E15.5 to E18.5 (Fig. 6E, F, K; Fig. S6A, B). Although the experimental data is noisy, the measured increase has a linear-like trend. To model the dynamics in this phase (Fig. 6K), we suppose that the basal cell layer is comprised of a single equipotent progenitor cell population, *b*, and a single non-proliferative suprabasal cell population, *s*, defined by the kinetics [46],

$$b \xrightarrow{\lambda} \begin{cases} b + b & \text{Pr. } 1 - r \\ s & \text{Pr. } r \end{cases}$$

so that at an overall rate λ, with probability $1 - r$, basal cells duplicate, while with probability r they commit to terminal differentiation and stratify into the suprabasal layer, i.e.

$$\dot{b} = \lambda(1-2r)b, \quad \dot{s} = \lambda r b$$

To ensure that suprabasal cells are produced in proportion to basal cells, $\dot{b} = \dot{s}$, i.e. $r = 1/3$. Further, if we propose that, over the three-day time course, the proliferation rate, λ, is approximately constant, we have that

$$b = b_0 e^{\lambda(t-t_0)/3} = s$$

where b_0 denotes the basal cell number at time $t_0 = 15.5$ days. With basal cell number increasing by approximately 2 over the three-day time course, this translates to a rate $\lambda = 0.7$ per day, similar to the estimated division rate during the early amplification phase (.

As a consistency check, we can question what would be the expected EdU incorporation rate in the basal cell layer. With an S-phase of around $t_s = 6-8$ hours, and a cell cycle time $1/\lambda$, we would expect a short-term EdU pulse to mark a fraction of $\lambda t_s \sim 0.8 \times (1/3) = 0.27$ of cells during the early phase. For a longer pulse (~3-4 hours), marked cells would have progressed through one round of division, leading to a doubling of the number to around 50 %. This Fig. is comparable to the measured estimates from the experimental data. In the later phase, the cell division rate drops by around 40 %, broadly consistent with the EdU measurements (Fig. 6H).

Figure Legends

Fig1. Centrioles, not cilia, are important for proper epidermal and hair follicle formation. (A) Gross phenotypes of control, centrosome mutant (*K14-Cre+; Sas-4$^{f/f}$*) and cilia mutant (*K14-Cre+; Ift88$^{f/f}$*) mice are shown at P21 (scale bar: 1 cm), as well as H&E histological staining of back-skin sections at P0 (scale bar: 100 μm). (B) Quantification of the interfollicular epidermal thickness in back-skin sections at P0. Control: 39 ± 4 μm (n = 8), *K14-Cre+; Sas-4$^{f/f}$*: 26 ± 2 μm (n = 8), *K14-Cre+; Ift88$^{f/f}$*: 40 ± 1 μm (n = 3). n is the number of animals per genotype in this and subsequent Fig.s.(C) Quantification of the number of hair follicles per mm in back-skin sections at P0. Control: 11 ± 1 (n = 5), *K14-Cre+; Sas4$^{f/f}$*: 4 ± 1 (n = 5), *K14-Cre+; Ift88$^{f/f}$*: 11 ± 1 (n = 3). **** $p < 0.0001$ (student's T-test or one-way ANOVA and Tukey's multiple comparisons test). Bars represent mean ± SD (standard deviation). (D) Representative images of control, *K14-Cre+; Sas-4$^{f/f}$* and *K14-Cre+; Ift88$^{f/f}$* back-skin sections at P0 stained for the epidermal layers' markers K14, K1 and Loricrin (LOR), the activation marker K6A (all green) and the basement membrane marker Integrin-α6 (ITGA6, red) (scale bar: 50 μm).

Fig2. The skin epidermal phenotypes in centrosome mutants are due to the activation of the mitotic surveillance pathway. (A) Representative images of control and *K14-Cre+; Sas-4$^{f/f}$* back-skin sections at E15.5 showing centrosome-marker (TUBG) loss, elevated levels of p53 and cell death (Cl.CASP3) in the mutant mice (scale bar: 20 μm). Dashed line represents the epidermal-dermal interface in all panels. (B) Quantification of the percentage of p53-positive nuclei in the back-skin basal epidermis at E15.5. Control: 3 ± 3 % (n = 5) and *K14-Cre+; Sas-4$^{f/f}$*: 37 ± 7 % (n = 5). (C) Quantification of Cl.CASP3-positive cells in the back-skin basal epidermis at E15.5. Control: 0.2 ± 0.1 % (n = 5) and *K14-Cre+; Sas-4$^{f/f}$*: 5 ± 2 % (n = 5). (D) Centrioles, besides providing the essential template for cilia, ensure efficient mitosis and repress the activation of the mitotic surveillance pathway: p53 stabilization mediated by 53BP1 and USP28 leading to cell death (mainly shown *in vivo*) or cell cycle arrest (mainly shown *in*

vitro). (E) Gross phenotypes of control, *K14-Cre+; Sas-4$^{f/f}$* (part of the same experiment in Fig. 1), *K14-Cre+; Sas-4$^{f/f}$; p53$^{f/f}$*; *K14-Cre+; Sas-4$^{f/f}$; 53bp1$^{em/em}$* and *K14-Cre+; Sas-4$^{f/f}$; Usp28$^{em/em}$* mice are shown at P21 (scale bar: 1 cm), as well as H&E histological staining of back-skin sections at P0 (scale bar: 100 µm). (F) Quantification of the interfollicular epidermal thickness in back-skin sections at P0. Control: 39 ± 4 µm (n = 8), *K14-Cre+; Sas-4$^{f/f}$*: 26 ± 2 µm (n = 8), *K14-Cre+; Sas-4$^{f/f}$; p53$^{f/f}$*: 40 ± 1 µm (n = 3), *K14-Cre+; Sas-4$^{f/f}$; 53bp1$^{em/em}$*: 42 ± 3 µm (n = 3), *K14-Cre+; Sas-4$^{f/f}$; Usp28$^{em/em}$*: 36 ± 3 µm (n = 5). Control and *K14-Cre+; Sas-4$^{f/f}$* animals are part of the same experiment in Fig. 1. (G) Quantification of the number of hair follicles per mm in back-skin sections at P0. Control: 11 ± 1 (n = 5), *K14-Cre+; Sas-4$^{f/f}$*: 4 ± 1 (n = 5), *K14-Cre+; Sas-4$^{f/f}$; p53$^{f/f}$*: 9 ± 1 (n = 3), *K14-Cre+; Sas-4$^{f/f}$; 53bp1$^{em/em}$*: 10 ± 1 (n = 3), *K14-Cre+; Sas-4$^{f/f}$; Usp28$^{em/em}$*: 10 ± 1 (n = 5). Controls and *K14-Cre+; Sas-4$^{f/f}$* are part of the same experiment in Fig. 1. * $p < 0.05$, ** $p < 0.01$, *** $p < 0.001$, **** $p < 0.0001$ (student's T-test or one-way ANOVA and Tukey's multiple comparisons test). Bars represent mean ± SD.

Fig3. The orientations of cell division do not correlate with differentiation in the developing centrosome mutant epidermis. (A) Representative images of parallel and perpendicular dividing basal cells in back-skin sections of the interfollicular basal layer of control at E16.5 (scale bar: 10 µm). (B) Radial histograms of the distribution of the angles of cell division orientation in late anaphase to telophase of basal epidermal cells at E16.5 in control (285 cells from 5 embryos) and *K14-Cre+; Sas-4$^{f/f}$; p53$^{f/f}$* (328 cells from 5 embryos) mice. Percentages of parallel (0 - 29°), oblique (30 - 59°) and perpendicular (60 - 90°) dividing basal layer cells at E16.5. Control: 42 ± 11 % (0 - 29°), 19 ± 9 % (30 – 59°), 40 ± 5 % (60 – 90°) and *K14-Cre+; Sas-4$^{f/f}$; p53$^{f/f}$*: 19 ± 4 % (0 – 29°), 21 ± 8 % (30 – 59°), 60 ± 11 % (60 – 90°). (C) Radial histograms of the distributions of the angles of cell division orientations in late anaphase to telophase of basal epidermal cells at E17.5 in control (231 cells from 5 embryos) and *K14-Cre+; Sas-4$^{f/f}$; p53$^{f/f}$* (421 cells from 5 embryos) mice. Percentages of parallel (0 - 29°), oblique

(30 - 59°) and perpendicular (60 - 90°) dividing basal layer cells at E17.5. Control: 47 ± 12 % (0 - 29°), 14 ± 6 % (30 – 59°), 39 ± 11 % (60 – 90°) and *K14-Cre+; Sas-4$^{f/f}$; p53$^{f/f}$*: 15 ± 6 % (0 – 29°), 27 ± 4 % (30 – 59°), 58 ± 8 % (60 – 90°). (D) Representative images of back-skin sections at E16.5 stained for K1 of control and *K14-Cre+; Sas-4$^{f/f}$; p53$^{f/f}$* mice (scale bar: 50 µm). Dashed line represents the epidermal-dermal interface in all panels. (E) Quantification of the differentiated (K1-positive) layer of back-skin sections at E16.5. Control: 24 ± 5 µm (n = 3) and *K14-Cre+; Sas-4$^{f/f}$; p53$^{f/f}$*: 23 ± 2 µm (n = 3). (F) Quantification of the density (cells per 100 µm) of basal layer cells of sagittal back-skin epidermal sections at E16.5. Control: 13 ± 0 (n=5) and *K14-Cre+; Sas-4$^{f/f}$; p53$^{f/f}$*: 16 ± 1 (n=5). n. s. = not significant, * $p < 0.05$, ** $p < 0.01$ (student's T-test). Angle measurements were compared using a two-way ANOVA, Kolmogorov-Smirnov Test and Chi squared Test, all of which gave similar statistical significance outcomes. Bars represent mean ± SD.

Fig4. Asymmetric cell division may not be essential for skin epidermal stratification and differentiation during development. (A) Representative images of control and MMC-treated skin explants at the indicated timepoints. Although proliferation (EdU and pHH3) was inhibited in the MMC-treated skin explants, cell differentiation (K10) was still possible (scale bar: 50 µm). Dashed line represents the epidermal-dermal interface in all panels. (B) Quantification of the K10-positive layer thickness in the control and MMC-treated skin explants. At E13.5, Control: 3 ± 2 µm (n = 6). At E14.5, Control: 29 ± 3 µm (n = 7), MMC-treated: 17 ± 4 µm (n = 7). At E15.5, Control: 33 ± 7 µm (n = 7), MMC-treated: 51 ± 14 µm (n = 12). (C) Quantification of the density (cells per 100 µm) of basal layer cells of control and MMC-treated skin explants. E13.5 control: 39 ± 5 (n = 7), E14.5 control: 23 ± 2 (n = 6), E14.5 MMC-treated: 15 ± 1 (n = 4), E15.5 control: 20 ± 4 (n = 6), and E15.5 MMC-treated: 6 ± 2 (n = 9). (D) Quantification of the density (cells per 100 µm) of suprabasal layer cells of control and MMC-treated skin explants. E13.5 control: 6 ± 5 (n = 7), E14.5 control: 36 ± 4 (n = 6), E14.5 MMC-treated: 21 ± 3 (n = 4), E15.5 control: 33 ± 9

(n = 6), and E15.5 MMC-treated: 22 ± 7 (n = 9). n.s. = not significant, * $p < 0.05$, ** $p < 0.01$, *** $p < 0.001$, **** $p < 0.0001$ (student's T-test or one-way ANOVA and Tukey's multiple comparisons test). Bars represent mean ± SD.

Fig5. The skin epidermal basal layer is more flexible during development. (A-C) Time-lapse images of the CAG::H2B-EGFP nuclear reporter in E13.5-E14.5 skin-roll explants taken every 7 minutes. (A, B) Examples of perpendicular dividing basal cells with daughter cells that point away from the epidermal-dermal interface that are either integrated into the basal layer after division (A, 26 out of 54 cells), or remain in the second layer for the duration of the analysis (B, 28 out of 54 cells). (C) An Example of a delaminating cell that leaves the basal layer, moves suprabasally and divides. (a total of 36 cells observed). Note the other dividing suprabasal cell (red asterisks) (scale bars: 10 μm). The data were obtained from 3 explants from 3 different embryos. Dashed line represents the epidermal-dermal interface in all panels. Yellow dots mark the cells of interest. (D) Representative images of back-skin sections at the indicated timepoints stained for the basement membrane zone marker Integrin-α6 (ITGA6, red) and the differentiation markers K10 or K1 (green) (scale bars: 10 μm).

Fig6. Skin epidermal stratification occurs in two phases.

(A-D) Quantification of the distances shown in (A). (B) crown-rump distance, (C) inter-limb distance and (D) orthogonal distance of wild-type embryos from E12.5-E18.5. Note the linear trend of the growth in the different directions. E12.5: n = 10, E13.5: n = 16, E14.5: n = 10, E15.5: n = 12, E16.5: n = 11, E17.5: n = 10 and E18.5: n = 4. (E, F) Cell densities (cells per 100 μm) of basal and suprabasal layer cells of sagittal back-skin sections of the epidermis from E12.5-E18.5 (n =5). The suprabasal cell density reaches parity with that of the basal cells starting at E15.5 (F). (G-J) Quantification of pHH3- (G) and EdU-positive (H) cells in the basal and suprabasal layers, with examples of the stainings shown at E14.5 (I, J; arrowheads) (scale

bar: 10 μm), from sagittal back-skin sections of the epidermis at the indicated timepoints (n = 5-6). (K) The exponential increase in total cell number between E12.5-E15.5 and the linear-trend increase between E15.5-E18.5, shown as the calculated total cell number from the measurements (total) and the model. * $p < 0.05$, ** $p < 0.01$, *** $p < 0.001$, **** $p < 0.0001$ (student's T-test). Bars represent mean ± SD.

Fig7. A proposed model of embryonic skin epidermal development. An illustration of the two phases of skin epidermal stratification. In the first phase between E13.5-E15.5, basal cells delaminate, both basal and suprabasal keratinocytes have high rates of cell division, where the angle of cell division orientation in the basal keratinocytes maybe uncoupled from epidermal stratification. In the second phase between E15.5-E18.5, proliferation rates are slower, decreasing dramatically in the suprabasal layer, and delamination maybe a dominant mechanism in maintaining stratification during tissue growth. The basal cells are outlined in red and the suprabasal cells are outlined in green.

Table 1: The measurements shown in Fig. 6. b = basal, sb = suprabasal, t = total.

	embryo growth			**cell density**			**mitotic index**		
	[mm]			**[cells/100µm]**			**pHH3 positive [%]**		**EdU positive [%]**
	crown-rump	limb distance	orthogonal		sagittal	transverse	sagittal	transverse	sagittal
E12.5	7.9 ± 0.2	2.0 ± 0.1	1.9 ± 0.1	b sb t	13 ± 1 2 ± 1 15 ± 1	17 ± 1 2 ± 0 19 ± 1	4 ± 1 5 ± 8 4 ± 1	3 ± 1 3 ± 3 3 ± 1	-
E13.5	9.9 ± 0.3	2.6 ± 0.2	2.8 ± 0.2	b sb t	14 ± 3 2 ± 1 16 ± 3	17 ± 2 2 ± 1 18 ± 2	4 ± 1 5 ± 5 4 ± 1	3 ± 1 10 ± 10 3 ± 1	63 ± 3 60 ± 3 62 ± 3
E14.5	11.5 ± 0.7	3.3 ± 0.4	3.2 ± 0.3	b sb t	17 ± 2 6 ± 2 23 ± 2	16 ± 1 6 ± 2 22 ± 3	4 ± 2 3 ± 3 4 ± 1	3 ± 1 4 ± 3 3 ± 1	52 ± 8 31 ± 8 40 ± 7
E15.5	13.5 ± 0.5	4 .2 ± 0.4	3.6 ± 0.4	b sb t	13 ± 1 13 ± 1 27 ± 2	15 ± 1 15 ± 1 29 ± 1	3 ± 0.5 1 ± 1 2 ± 0.5	5 ± 1 1 ± 1 3 ± 1	46 ± 7 14 ± 5 25 ± 4
E16.5	15.1 ± 0.5	4.3 ± 0.4	4.2 ± 0.3	b sb t	13 ± 0 13 ± 2 26 ± 2	15 ± 1 14 ± 2 29 ± 2	3 ± 2 0 ± 0 2 ± 1	4 ± 3 0.2 ± 0.5 2 ± 2	40 ± 8 11 ± 6 20 ± 6
E17.5	19.3 ± 0.6	5.5 ± 0.5	5.6 ± 0.3	b sb t	14 ± 1 10 ± 1 24 ± 1	15 ± 1 15 ± 2 30 ± 3	2 ± 2 0 ± 0 1 ± 1	3 ± 2 1 ± 1 2 ± 1	-
E18.5	20.0 ± 0.5	5.7 ± 0.6	5.9 ± 0.4	b sb t	13 ± 1 12 ± 3 26 ± 3	12 ± 1 11 ± 2 23 ± 3	2 ± 2 1 ± 1 2 ± 2	2 ± 2 0 ± 0 1 ± 1	-

Supplementary Figure Legends

FigS1. Growth, hair follicle and mild barrier defects upon centriole loss in stratified epithelia including the skin epidermis. (A) Representative images of control and *K14-Cre+; Sas-4$^{f/f}$* back-skin sections at E15.5 showing centrosome-markers loss (TUGB and CEP164) (scale bar: 10 μm). Dashed line represents the epidermal-dermal interface in all panels. (B) Quantification of centrosome-containing cells in back-skin sections at E15.5 of control and *K14-Cre+; Sas-4$^{f/f}$* mice. Control: 87 ± 3 % (basal), 72 ± 7 % (suprabasal) and *K14-Cre+; Sas-4$^{f/f}$*: 5 ± 2 % (basal), 3 ± 2 % (suprabasal) (n = 5). (C) Quantification of the weight difference between control (n = 7) and *K14-Cre+; Sas-4$^{f/f}$* (n = 6) mice from P0 to P20. (D) Toluidine Blue dye-penetration assay of control and *K14-Cre+; Sas-4$^{f/f}$* embryos at E17.5 and E18.5. Arrowheads indicate regions with delayed barrier formation in *K14-Cre+; Sas-4$^{f/f}$* embryos (scale bar: 2 mm). (E) Representative images of control and *K14-Cre+; Ift88$^{f/f}$* back-skin sections at E15.5 showing cilia-marker (ARL13B) loss (scale bar: 10 μm). Dashed line represents the epidermal-dermal interface in all panels. (F) Quantification of ciliated cells in back-skin sections at E15.5 of control and *K14-Cre+; Ift88$^{f/f}$* mice. Control: 84 ± 4 (basal), 24 ± 8 (suprabasal) and *K14-Cre+; Ift88$^{f/f}$*: 11 ± 3 (basal), 3 ± 2 (suprabasal) (n = 5). * $p < 0.05$, ** $p < 0.01$, *** $p < 0.001$, **** $p < 0.0001$ (student's T-test). Bars represent mean ± SD. (G) H&E histological stainings of back-skin sections at P8 of control, *K14-Cre+; Sas-4$^{f/f}$* and *K14-Cre+; Ift88$^{f/f}$* mice (scale bar: 100 μm).

FigS2. p53, cell death, cell cycle and residual proteins in different mutants. (A) Representative images of control and *K14-Cre+; Ift88$^{f/f}$* back-skin sections at E15.5 showing no detectable p53 upregulation in cilia mutants (scale bar = 20 μm). TUBG marks the centrosomes. Dashed line represents the epidermal-dermal interface in all panels. (B) Representative images of control and *K14-Cre+; Sas-4$^{f/f}$* back-skin sections at P0 showing high levels of nuclear p53 and rare cell death (Cl.CASP3) in the mutant mice (scale bar: 20 μm). TUBG marks the centrosomes. Dashed line represents the epidermal-dermal interface in all panels. (C)

Quantification of the percentage of p53-positive nuclei in the back-skin basal epidermis at P0. Control: 4 ± 2 % (n = 5) and *K14-Cre+; Sas-4$^{f/f}$*: 58 ± 7 % (n = 5). (D) Quantification of Cl.CASP3-positive cells in the back-skin basal epidermis at P0. Control: 0.0006 ± 0.0009 % (n = 5) and *K14-Cre+; Sas-4$^{f/f}$*: 0.007 ± 0.004 % (n = 5). (E) Cell cycle profiles of isolated primary keratinocytes at P0. Control (n = 5): 77 ± 3 % (G1), 19 ± 2 % (S), 8 ± 2 % (G2/M); and *K14-Cre+; Sas-4$^{f/f}$* (n = 4): 73 ± 6 % (G1), 18 ± 2 % (S), 12 ± 4 % (G2/M). (F) Quantification of the percentage of pHH3-positive cells in the basal layer of back-skin epidermal sections at E15.5. Control: 3 ± 0.4 % (n = 5), *K14-Cre+; Sas-4$^{f/w}$; p53$^{f/f}$*: 3 ± 1 % (n = 5), *K14-Cre+; Sas-4$^{f/f}$*: 6 ± 2 % (n = 5) and *K14-Cre+; Sas-4$^{f/f}$; p53$^{f/f}$*: 7 ± 2 % (n = 4). n. s. = not significant, * $p < 0.05$, **** $p < 0.0001$ (student's T-test). Bars represent mean ± SD. (G, H) Representative images of back-skin epidermal sections at P0 of control and *K14-Cre+; Sas-4$^{f/f}$; 53bp1$^{em/em}$* (G) and *K14-Cre+; Sas-4$^{f/f}$; Usp28$^{em/em}$* (H) mice, showing residual signal of 53BP1 (G) or USP28 (H) suggesting hypomorphic alleles (scale bars: 50 µm).

FigS3. Control genotypes for the cell division angle measurements and cell density in the basal layer, and assessment of proliferation in centrosome and cilia mutants (A) Radial histogram distribution of the angles of cell division in late anaphase to telophase of basal epidermal cells at E16.5. *K14-Cre+; Sas4$^{f/w}$; p53$^{f/f}$*: 119 cells from 5 embryos. (B) Percentages of parallel (0 - 29°), oblique (30 - 59°) and perpendicular (60 - 90°) dividing cells in basal layer cells at E16.5. Control: 42 ± 11 % (0 - 29°), 19 ± 9 % (30 – 59°), 40 ± 5 % (60 – 90°), *K14-Cre+; Sas-4$^{f/w}$; p53$^{f/f}$*: 37 ± 11 % (0 – 29°), 18 ± 5 % (30 – 59°), 44 ± 7 % (60 – 90°) and *K14-Cre+; Sas-4$^{f/f}$; p53$^{f/f}$*: 19 ± 4 % (0 – 29°), 21 ± 8 % (30 – 59°), 60 ± 11 % (60 – 90°) (n = 5). (C) Percentages of parallel (0-44°) and perpendicular (45-90°) dividing cells in basal layer cells at E16.5. Control: 53 ± 9 % (0 - 44°), 47 ± 9 % (45 – 90°), *K14-Cre+; Sas-4$^{f/w}$; p53$^{f/f}$*: 48 ± 8 % (0 – 44°), 52 ± 8 % (45 – 90°) and *K14-Cre+; Sas-4$^{f/f}$; p53$^{f/f}$*: 28 ± 11 % (0 – 44°), 72 ± 11 % (45 – 90°) (n = 5). (D) Quantification of the density (cells per 100 µm) of basal layer cells of back-skin

sections of the epidermis at E16.5. Control: 13 ± 0, K14-Cre+; *Sas-4$^{f/w}$; p53$^{f/f}$*: 14 ± 1 and *K14-Cre+; Sas-4$^{f/f}$; p53$^{f/f}$*: 16 ± 1 (n = 5). (E) Quantification of the percentage of the EdU-positive cells in the basal layer of back-skin epidermal sections at E16.5. Control: 40 ± 8, K14-Cre+ (n = 6); *K14-Cre+; Sas-4$^{f/w}$; p53$^{f/f}$*: 48 ± 5 (n = 5); *K14-Cre+; Ift88$^{f/f}$:* 43 ± 5 (n = 6) and *K14-Cre+; Sas-4$^{f/f}$; p53$^{f/f}$*: 49 ± 6 (n =5). n. s. = not significant, * p < 0.05, ** p < 0.01 (student's T-test). Bars represent mean ± SD.

FigS4. MMC-treated skin explants showed widespread cell death. Representative images of control and MMC-treated skin explants. MMC-treated explants showed elevated levels of cell death (Cl.CASP3) particularly at E14.5 (scale bar: 50 μm). Dashed line represents the epidermal-dermal interface in all panels.

FigS5. The skin explants on filters (flat) and as rolls. (A) Representative image of the CAG::H2B-EGFP reporter taken from the time-lapses of flat skin explants at E14.5 shown in the XY (yellow lines) and Z dimensions (scale bars: 10 μm). (B, C) Representative images of the skin explant rolls (B), used for time-lapse imaging, and the flat skin explants (C) at E13.5-E15.5 stained for the basement membrane zone marker Integrin-α6 (ITGA6, red) and the differentiation marker K10 (green) (scale bar: 50 μm).

FigS6. Cell number and mitotic index measurements in the transverse direction. (A, B) Quantification of the cell density (A and B, cells per 100 μm) and pHH3-positive cells (C) of basal and suprabasal layer cells of transverse back-skin sections of the epidermis from E12.5-E18.5 (n =5). The suprabasal cell density reaches parity with that of the basal cells starting at E15.5 (B).

References

1 Byrne, C., Hardman, M. & Nield, K. Covering the limb--formation of the integument. *Journal of anatomy* **202**, 113-124, doi:10.1046/J.1469-7580.2003.00142.X (2003).

2 Smart, I. H. Variation in the plane of cell cleavage during the process of stratification in the mouse epidermis. *Br J Dermatol* **82**, 276-282, doi:10.1111/j.1365-2133.1970.tb12437.x (1970).

3 Koster, M. I. & Roop, D. R. The role of p63 in development and differentiation of the epidermis. *J Dermatol Sci* **34**, 3-9, doi:10.1016/j.jdermsci.2003.10.003 (2004).

4 Mills, A. A. *et al.* p63 is a p53 homologue required for limb and epidermal morphogenesis. *Nature* **398**, 708-713, doi:10.1038/19531 (1999).

5 Hammond, N. L., Dixon, J. & Dixon, M. J. Periderm: Life-cycle and function during orofacial and epidermal development. *Semin Cell Dev Biol* **91**, 75-83, doi:10.1016/j.semcdb.2017.08.021 (2019).

6 Blanpain, C., Lowry, W. E., Pasolli, H. A. & Fuchs, E. Canonical notch signaling functions as a commitment switch in the epidermal lineage. *Genes Dev* **20**, 3022-3035, doi:10.1101/gad.1477606 (2006).

7 Hardman, M. J., Sisi, P., Banbury, D. N. & Byrne, C. Patterned acquisition of skin barrier function during development. *Development* **125**, 1541-1552 (1998).

8 Dotto, G. P. Signal transduction pathways controlling the switch between keratinocyte growth and differentiation. *Crit Rev Oral Biol Med* **10**, 442-457, doi:10.1177/10454411990100040201 (1999).

9 Nowak, J. A., Polak, L., Pasolli, H. A. & Fuchs, E. Hair follicle stem cells are specified and function in early skin morphogenesis. *Cell Stem Cell* **3**, 33-43, doi:10.1016/j.stem.2008.05.009 (2008).

10 Poulson, N. D. & Lechler, T. Asymmetric cell divisions in the epidermis. *Int Rev Cell Mol Biol* **295**, 199-232, doi:10.1016/B978-0-12-394306-4.00012-5 (2012).

11 Lechler, T. & Fuchs, E. Asymmetric cell divisions promote stratification and differentiation of mammalian skin. *Nature* **437**, 275-280, doi:10.1038/nature03922 (2005).

12 Williams, S. E., Beronja, S., Pasolli, H. A. & Fuchs, E. Asymmetric cell divisions promote Notch-dependent epidermal differentiation. *Nature* **470**, 353-358, doi:10.1038/nature09793 (2011).

13 Vorhagen, S. & Niessen, C. M. Mammalian aPKC/Par polarity complex mediated regulation of epithelial division orientation and cell fate. *Exp Cell Res* **328**, 296-302, doi:10.1016/j.yexcr.2014.08.008 (2014).

14 Xie, W. & Zhou, J. Regulation of mitotic spindle orientation during epidermal stratification. *J Cell Physiol* **232**, 1634-1639, doi:10.1002/jcp.25750 (2017).

15 Seldin, L., Muroyama, A. & Lechler, T. NuMA-microtubule interactions are critical for spindle orientation and the morphogenesis of diverse epidermal structures. *Elife* **5**, doi:10.7554/eLife.12504 (2016).

16 Schatten, H. & Sun, Q. Y. Functions and dysfunctions of the mammalian centrosome in health, disorders, disease, and aging. *Histochem Cell Biol* **150**, 303-325, doi:10.1007/s00418-018-1698-1 (2018).

17 Carvalho-Santos, Z. *et al.* Stepwise evolution of the centriole-assembly pathway. *Journal of cell science* **123**, 1414-1426, doi:10.1242/jcs.064931 (2010).

18 Bond, J. *et al.* A centrosomal mechanism involving CDK5RAP2 and CENPJ controls brain size. *Nature Genetics* **37**, 353-355, doi:10.1038/ng1539 (2005).

19 Bazzi, H. & Anderson, K. V. Acentriolar mitosis activates a p53-dependent apoptosis pathway in the mouse embryo. *Proc Natl Acad Sci U S A* **111**, E1491-1500, doi:10.1073/pnas.1400568111 (2014).

20 Insolera, R., Bazzi, H., Shao, W., Anderson, K. V. & Shi, S. H. Cortical neurogenesis in the absence of centrioles. *Nat Neurosci* **17**, 1528-1535, doi:10.1038/nn.3831 (2014).

21 Lambrus, B. G. *et al.* p53 protects against genome instability following centriole duplication failure. *J Cell Biol* **210**, 63-77, doi:10.1083/jcb.201502089 (2015).
22 Wong, Y. L. *et al.* Cell biology. Reversible centriole depletion with an inhibitor of Polo-like kinase 4. *Science* **348**, 1155-1160, doi:10.1126/science.aaa5111 (2015).
23 Fong, C. S. *et al.* 53BP1 and USP28 mediate p53-dependent cell cycle arrest in response to centrosome loss and prolonged mitosis. *Elife* **5**, doi:10.7554/eLife.16270 (2016).
24 Lambrus, B. G. *et al.* A USP28-53BP1-p53-p21 signaling axis arrests growth after centrosome loss or prolonged mitosis. *J Cell Biol* **214**, 143-153, doi:10.1083/jcb.201604054 (2016).
25 Meitinger, F. *et al.* 53BP1 and USP28 mediate p53 activation and G1 arrest after centrosome loss or extended mitotic duration. *J Cell Biol* **214**, 155-166, doi:10.1083/jcb.201604081 (2016).
26 Lambrus, B. G. & Holland, A. J. A New Mode of Mitotic Surveillance. *Trends Cell Biol* **27**, 314-321, doi:10.1016/j.tcb.2017.01.004 (2017).
27 Fish, J. L., Kosodo, Y., Enard, W., Pääbo, S. & Huttner, W. B. Aspm specifically maintains symmetric proliferative divisions of neuroepithelial cells. *Proceedings of the National Academy of Sciences of the United States of America* **103**, 10438-10443, doi:10.1073/pnas.0604066103 (2006).
28 Haycraft, C. J. *et al.* Intraflagellar transport is essential for endochondral bone formation. *Development* **134**, 307-316, doi:10.1242/dev.02732 (2007).
29 Croyle, M. J. *et al.* Role of epidermal primary cilia in the homeostasis of skin and hair follicles. *Development* **138**, 1675-1685, doi:10.1242/dev.060210 (2011).
30 Ezratty, E. J. *et al.* A role for the primary cilium in Notch signaling and epidermal differentiation during skin development. *Cell* **145**, 1129-1141, doi:10.1016/j.cell.2011.05.030 (2011).
31 Hafner, M. *et al.* Keratin 14 Cre Transgenic Mice Authenticate Keratin 14 as an Oocyte-Expressed Protein. *Genesis* **38**, 176-181, doi:10.1002/gene.20016 (2004).
32 Mikule, K. *et al.* Loss of centrosome integrity induces p38-p53-p21-dependent G1-S arrest. *Nat Cell Biol* **9**, 160-170 (2007).
33 Williams, S. E., Ratliff, L. A., Postiglione, M. P., Knoblich, J. A. & Fuchs, E. Par3-mInsc and Galphai3 cooperate to promote oriented epidermal cell divisions through LGN. *Nat Cell Biol* **16**, 758-769, doi:10.1038/ncb3001 (2014).
34 Kashiwagi, M., Kuroki, T. & Huh, N. Specific inhibition of hair follicle formation by epidermal growth factor in an organ culture of developing mouse skin. *Dev Biol* **189**, 22-32, doi:10.1006/dbio.1997.8650 (1997).
35 Gupta, K. *et al.* Single-Cell Analysis Reveals a Hair Follicle Dermal Niche Molecular Differentiation Trajectory that Begins Prior to Morphogenesis. *Dev Cell* **48**, 17-31.e16, doi:10.1016/j.devcel.2018.11.032 (2019).
36 Mok, K. W. *et al.* Dermal Condensate Niche Fate Specification Occurs Prior to Formation and Is Placode Progenitor Dependent. *Developmental Cell*, doi:10.1016/j.devcel.2018.11.034 (2019).
37 Moriyama, M. *et al.* Multiple roles of Notch signaling in the regulation of epidermal development. *Dev Cell* **14**, 594-604, doi:10.1016/j.devcel.2008.01.017 (2008).
38 Kantaputra, P. *et al.* The smallest teeth in the world are caused by mutations in the PCNT gene. *Am J Med Genet A* **155A**, 1398-1403, doi:10.1002/ajmg.a.33984 (2011).
39 Qvist, P. *et al.* CtIP Mutations Cause Seckel and Jawad Syndromes. *PLoS genetics* **7**, e1002310, doi:10.1371/journal.pgen.1002310 (2011).
40 Cui, R. *et al.* Central role of p53 in the suntan response and pathologic hyperpigmentation. *Cell* **128**, 853-864, doi:10.1016/j.cell.2006.12.045 (2007).
41 Goetz, S. C. & Anderson, K. V. The primary cilium: a signalling centre during vertebrate development. *Nat Rev Genet* **11**, 331-344, doi:nrg2774 [pii]

10.1038/nrg2774 (2010).
42 Pan, Y. *et al.* gamma-secretase functions through Notch signaling to maintain skin appendages but is not required for their patterning or initial morphogenesis. *Dev Cell* **7**, 731-743, doi:10.1016/j.devcel.2004.09.014 (2004).
43 Watt, F. M. & Fujiwara, H. Cell-extracellular matrix interactions in normal and diseased skin. *Cold Spring Harb Perspect Biol* **3**, doi:10.1101/cshperspect.a005124 (2011).
44 Morrow, A., Underwood, J., Seldin, L., Hinnant, T. & Lechler, T. Regulated spindle orientation buffers tissue growth in the epidermis. *Elife* **8**, doi:10.7554/eLife.48482 (2019).
45 Yuspa, S. H. & Harris, C. C. Altered differentiation of mouse epidermal cells treated with retinyl acetate in vitro. *Exp Cell Res* **86**, 95-105, doi:10.1016/0014-4827(74)90653-3 (1974).
46 Mesa, K. R. *et al.* Homeostatic Epidermal Stem Cell Self-Renewal Is Driven by Local Differentiation. *Cell Stem Cell* **23**, 677-686.e674, doi:10.1016/j.stem.2018.09.005 (2018).
47 Miroshnikova, Y. A. *et al.* Adhesion forces and cortical tension couple cell proliferation and differentiation to drive epidermal stratification. *Nat Cell Biol* **20**, 69-80, doi:10.1038/s41556-017-0005-z (2018).
48 Clayton, E. *et al.* A single type of progenitor cell maintains normal epidermis. *Nature* **446**, 185-189, doi:10.1038/nature05574 (2007).
49 Box, K., Joyce, B. W. & Devenport, D. Epithelial geometry regulates spindle orientation and progenitor fate during formation of the mammalian epidermis. *Elife* **8**, doi:10.7554/eLife.47102 (2019).
50 Williams, S. E. & Fuchs, E. Oriented divisions, fate decisions. *Curr Opin Cell Biol* **25**, 749-758, doi:10.1016/j.ceb.2013.08.003 (2013).
51 Lefort, K. & Dotto, G. P. Notch signaling in the integrated control of keratinocyte growth/differentiation and tumor suppression. *Semin Cancer Biol* **14**, 374-386, doi:10.1016/j.semcancer.2004.04.017 (2004).
52 Watt, F. M., Estrach, S. & Ambler, C. A. Epidermal Notch signalling: differentiation, cancer and adhesion. *Curr Opin Cell Biol* **20**, 171-179, doi:10.1016/j.ceb.2008.01.010 (2008).
53 Jacks, T. *et al.* Tumor spectrum analysis in p53-mutant mice. *Curr Biol* **4**, 1-7 (1994).
54 Hadjantonakis, A. K. & Papaioannou, V. E. Dynamic in vivo imaging and cell tracking using a histone fluorescent protein fusion in mice. *BMC Biotechnol* **4**, 33 (2004).
55 Rübsam, M. *et al.* E-cadherin integrates mechanotransduction and EGFR signaling to control junctional tissue polarization and tight junction positioning. *Nature Communications* **8**, 1250, doi:10.1038/s41467-017-01170-7 (2017).
56 DiTommaso, T. & Foijer, F. Barrier Function Assay. *Bio-protocol* **4**, e1133, doi:10.21769/BioProtoc.1133 (2014).

Figure 1

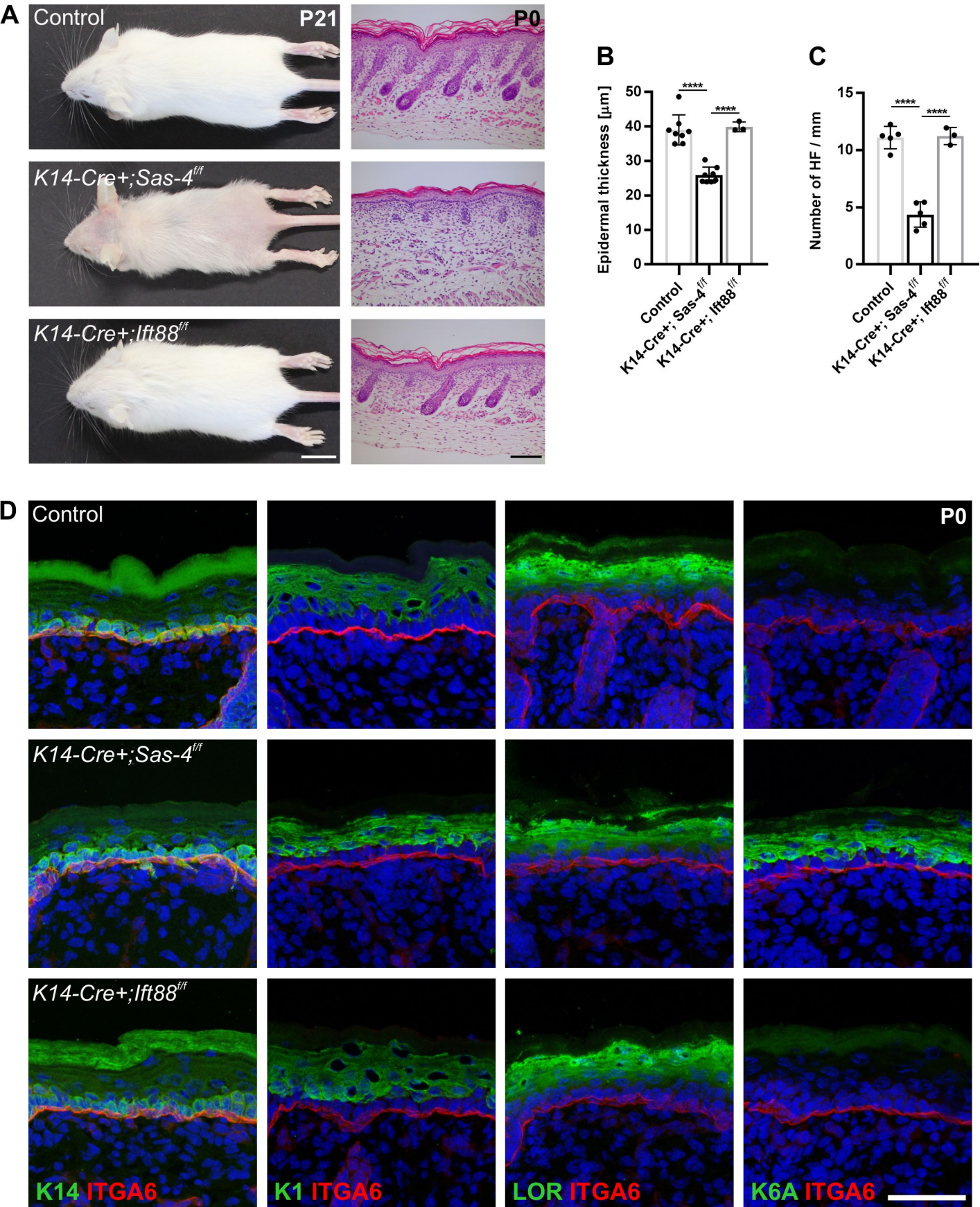
A
Control
P21
P0
K14-Cre+;Sas-4f/f
K14-Cre+;Ift88f/f
B
Epidermal thickness [µm]
50
40
30
20
10
0
****
****
Control
K14-Cre+; Sas-4f/f
K14-Cre+; Ift88f/f
C
Number of HF / mm
15
10
5
0
****
****
Control
K14-Cre+; Sas-4f/f
K14-Cre+; Ift88f/f
D
Control
P0
K14-Cre+;Sas-4f/f
K14-Cre+;Ift88f/f
K14 ITGA6
K1 ITGA6
LOR ITGA6
K6A ITGA6

Figure 2

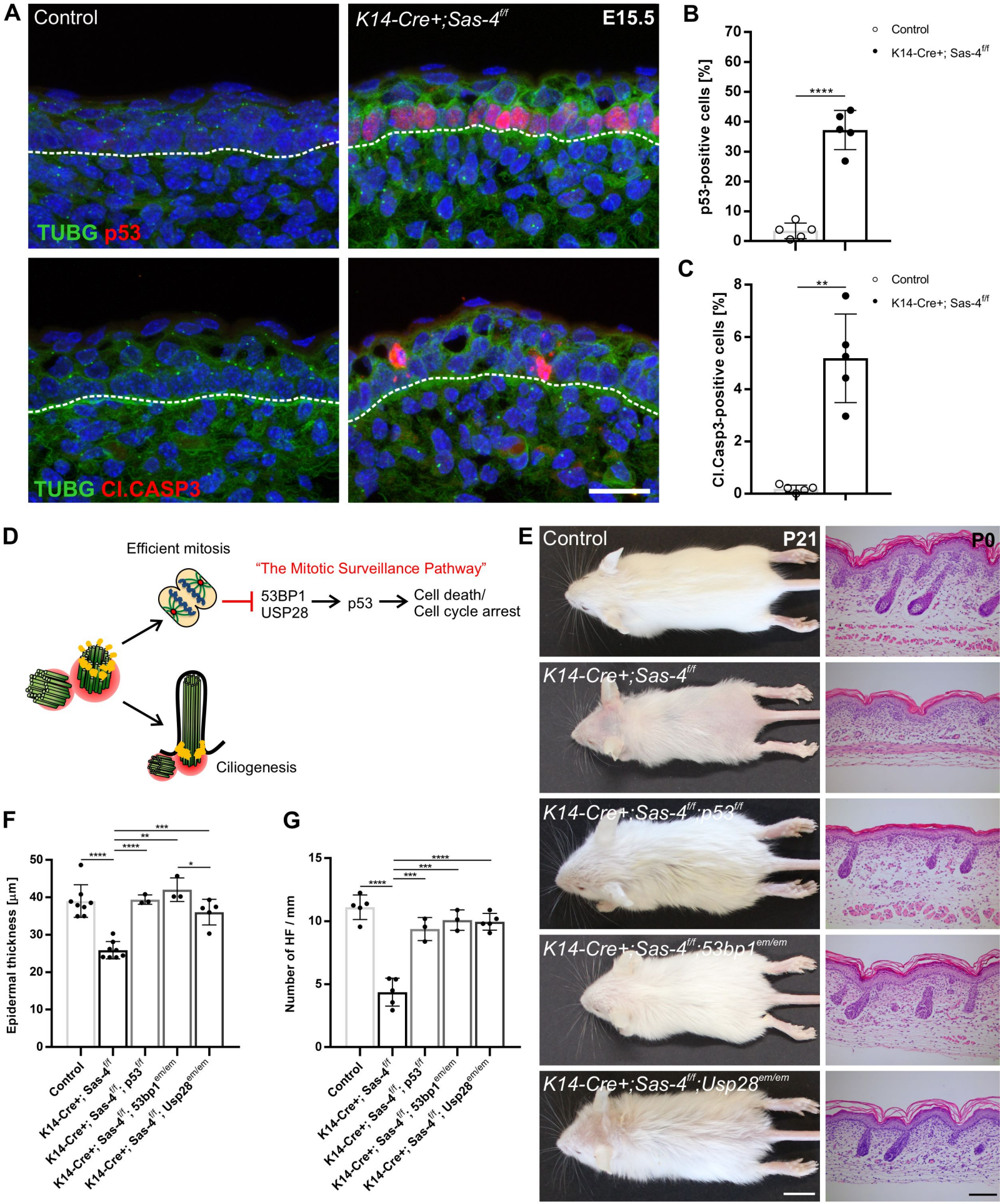
A
Control
K14-Cre+;Sas-4f/f
E15.5
TUBG p53
TUBG Cl.CASP3
B
p53-positive cells [%]
Control
K14-Cre+; Sas-4f/f
****
C
Cl.Casp3-positive cells [%]
Control
K14-Cre+; Sas-4f/f
**
D
Efficient mitosis
"The Mitotic Surveillance Pathway"
53BP1
USP28
p53
Cell death/
Cell cycle arrest
Ciliogenesis
E
Control
P21
P0
K14-Cre+;Sas-4f/f
K14-Cre+;Sas-4f/f;p53f/f
K14-Cre+;Sas-4f/f;53bp1em/em
K14-Cre+;Sas-4f/f;Usp28em/em
F
Epidermal thickness [µm]
G
Number of HF / mm
Control
K14-Cre+; Sas-4f/f
K14-Cre+; Sas-4f/f; p53f/f
K14-Cre+; Sas-4f/f; 53bp1em/em
K14-Cre+; Sas-4f/f; Usp28em/em

Figure 3

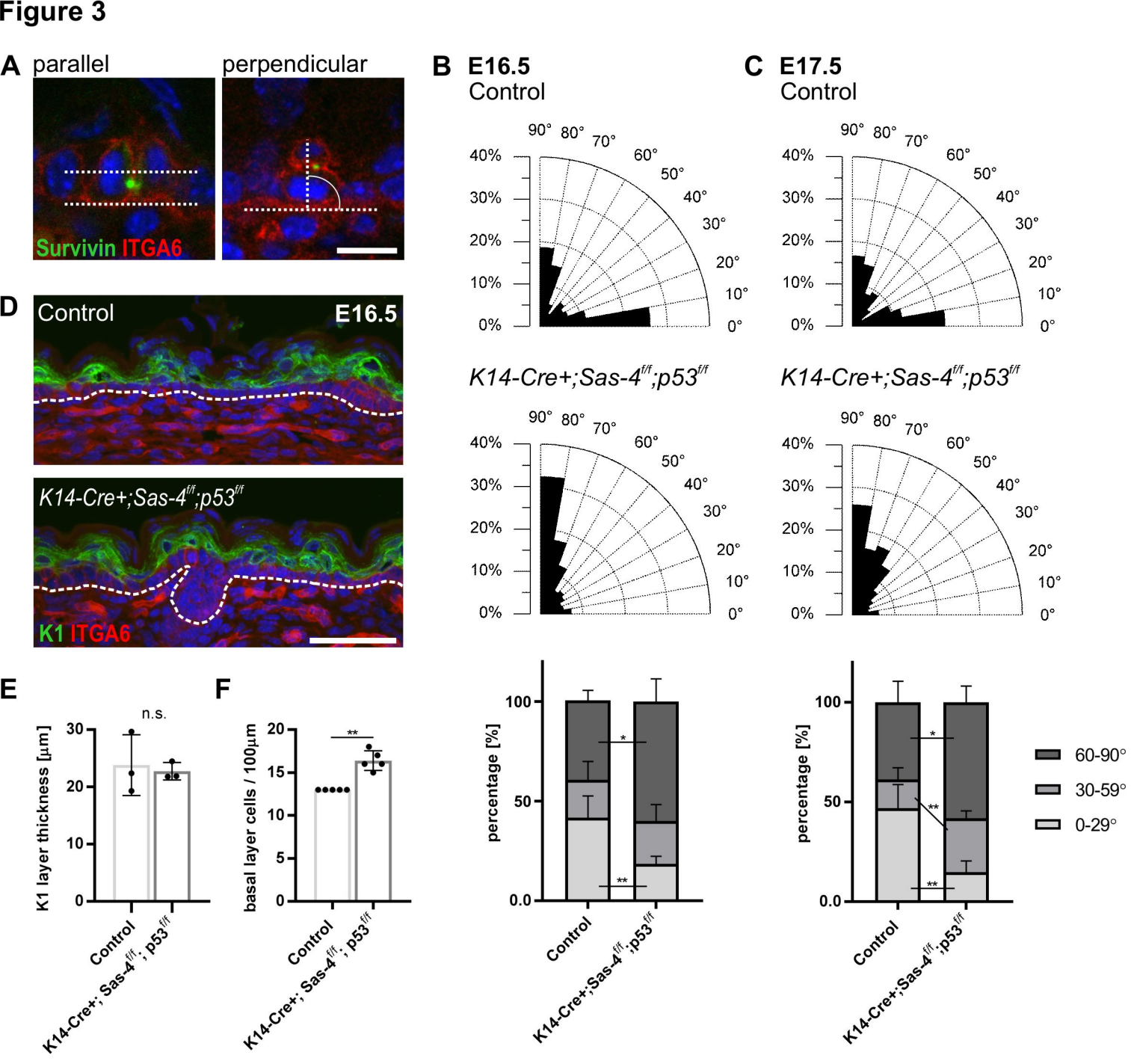
A
parallel
perpendicular
Survivin ITGA6
B
E16.5
Control
C
E17.5
Control
90° 80° 70° 60° 50° 40° 30° 20° 10° 0°
40% 30% 20% 10% 0%
K14-Cre+;Sas-4f/f;p53f/f
D
Control
E16.5
K14-Cre+;Sas-4f/f;p53f/f
K1 ITGA6
E
K1 layer thickness [µm]
n.s.
30 20 10 0
Control
K14-Cre+; Sas-4f/f; p53f/f
F
basal layer cells / 100µm
**
20 15 10 5 0
Control
K14-Cre+; Sas-4f/f; p53f/f
percentage [%]
100 50 0.0
*
**
Control
K14-Cre+;Sas-4f/f;p53f/f
60-90°
30-59°
0-29°

Figure 4

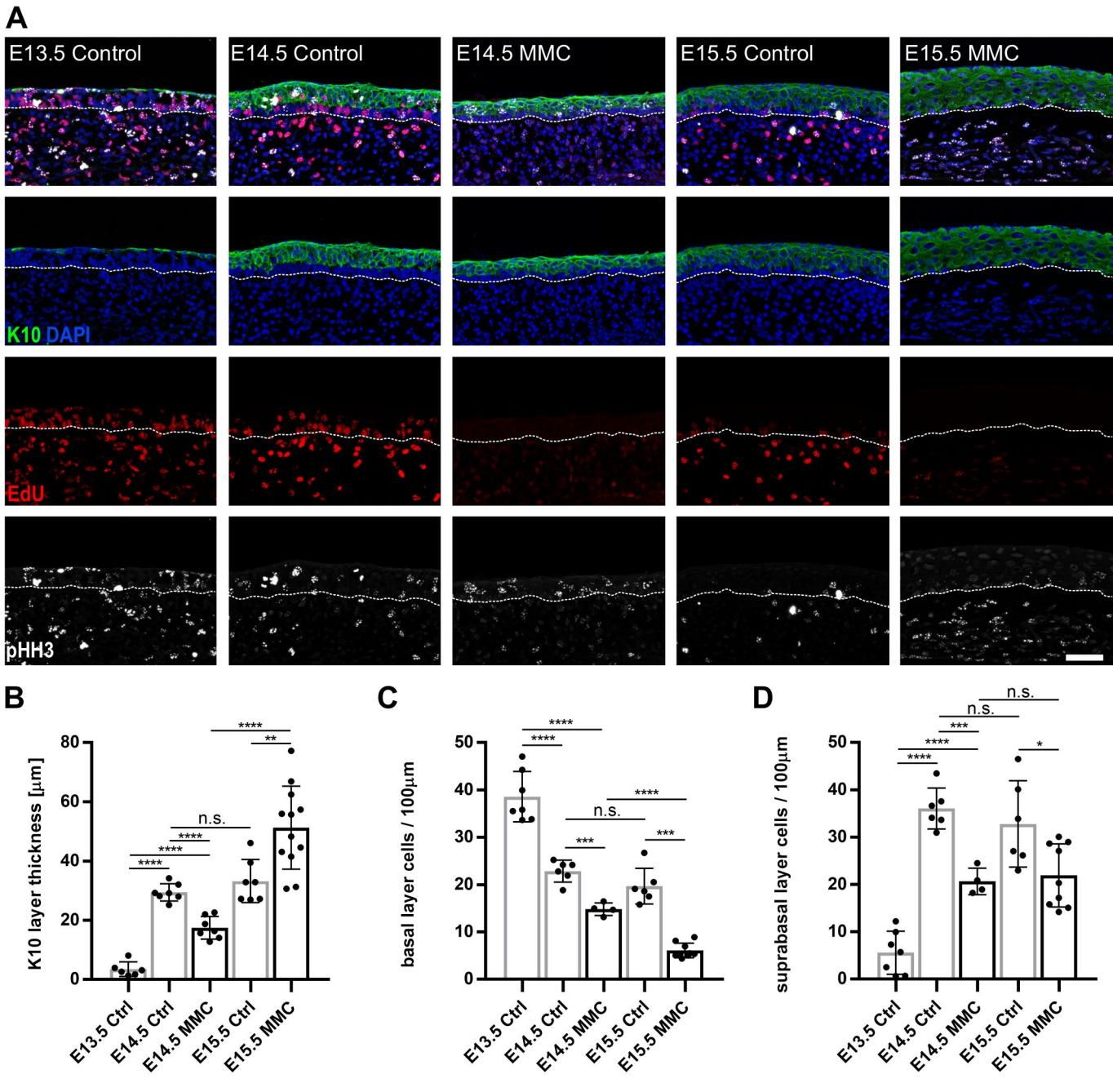
A
E13.5 Control
E14.5 Control
E14.5 MMC
E15.5 Control
E15.5 MMC
K10 DAPI
EdU
pHH3
B
K10 layer thickness [µm]
0
20
40
60
80
****
**
n.s.
****
****
****
E13.5 Ctrl
E14.5 Ctrl
E14.5 MMC
E15.5 Ctrl
E15.5 MMC
C
basal layer cells / 100µm
0
10
20
30
40
50
****
****
n.s.
****
***
***
E13.5 Ctrl
E14.5 Ctrl
E14.5 MMC
E15.5 Ctrl
E15.5 MMC
D
suprabasal layer cells / 100µm
0
10
20
30
40
50
n.s.
n.s.
***
****
****
*
E13.5 Ctrl
E14.5 Ctrl
E14.5 MMC
E15.5 Ctrl
E15.5 MMC

Figure 5

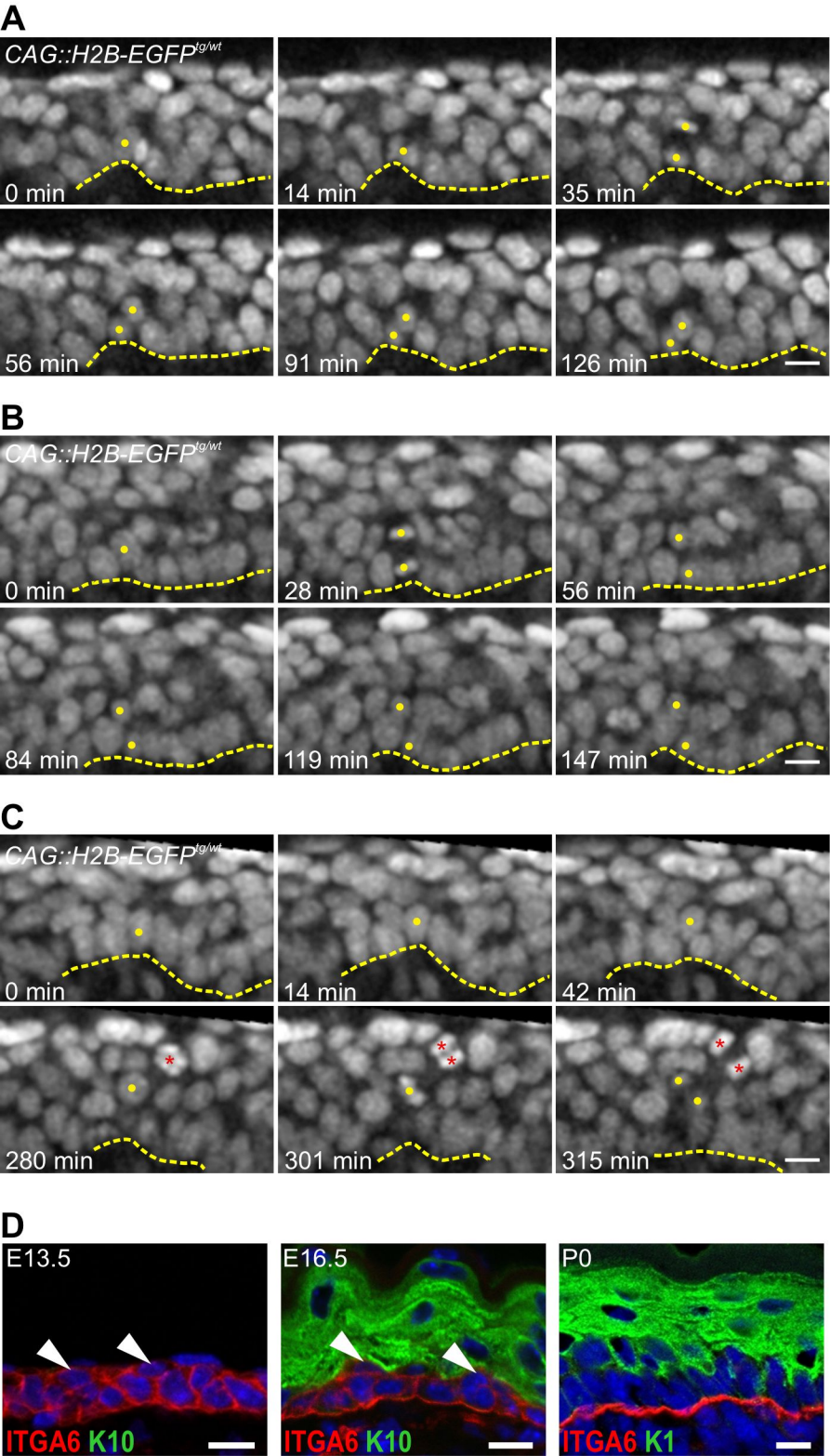
A
CAG::H2B-EGFP tg/wt
0 min
14 min
35 min
56 min
91 min
126 min
B
CAG::H2B-EGFP tg/wt
0 min
28 min
56 min
84 min
119 min
147 min
C
CAG::H2B-EGFP tg/wt
0 min
14 min
42 min
280 min
301 min
315 min
D
E13.5
E16.5
P0
ITGA6 K10
ITGA6 K10
ITGA6 K1

Figure 6

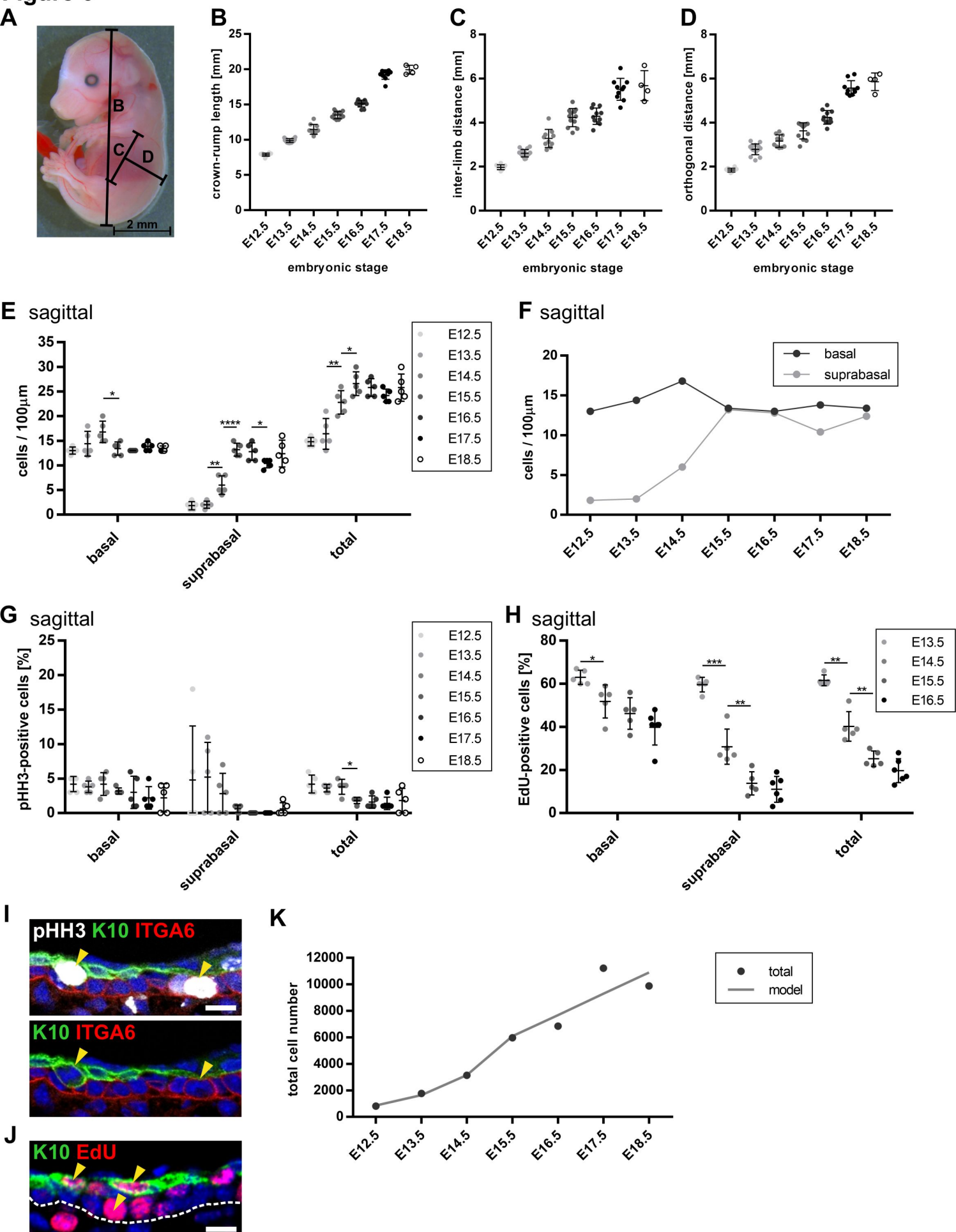
A
B
C
D
2 mm
B
crown-rump length [mm]
embryonic stage
C
inter-limb distance [mm]
embryonic stage
D
orthogonal distance [mm]
embryonic stage
E12.5
E13.5
E14.5
E15.5
E16.5
E17.5
E18.5
E sagittal
cells / 100µm
basal
suprabasal
total
F sagittal
basal
suprabasal
G sagittal
pHH3-positive cells [%]
H sagittal
EdU-positive cells [%]
I
pHH3 K10 ITGA6
K10 ITGA6
J
K10 EdU
K
total cell number
total
model

Figure 7

First Phase

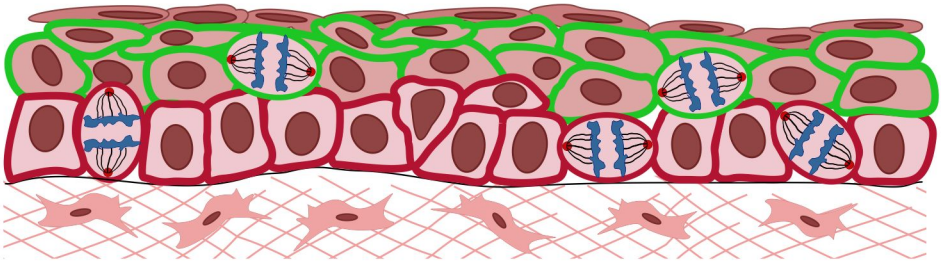

Second Phase

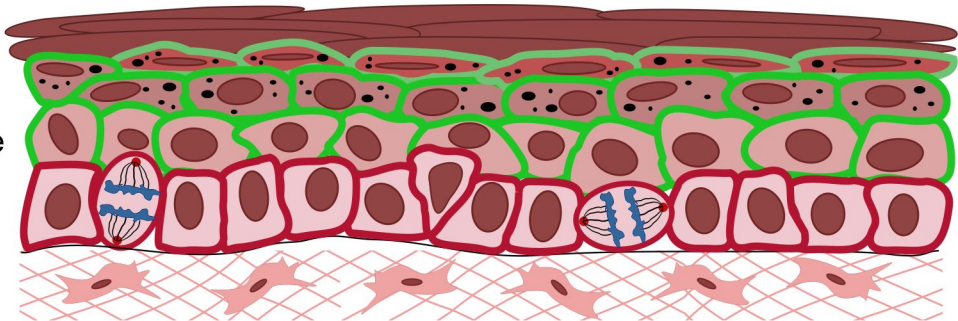

Figure S1

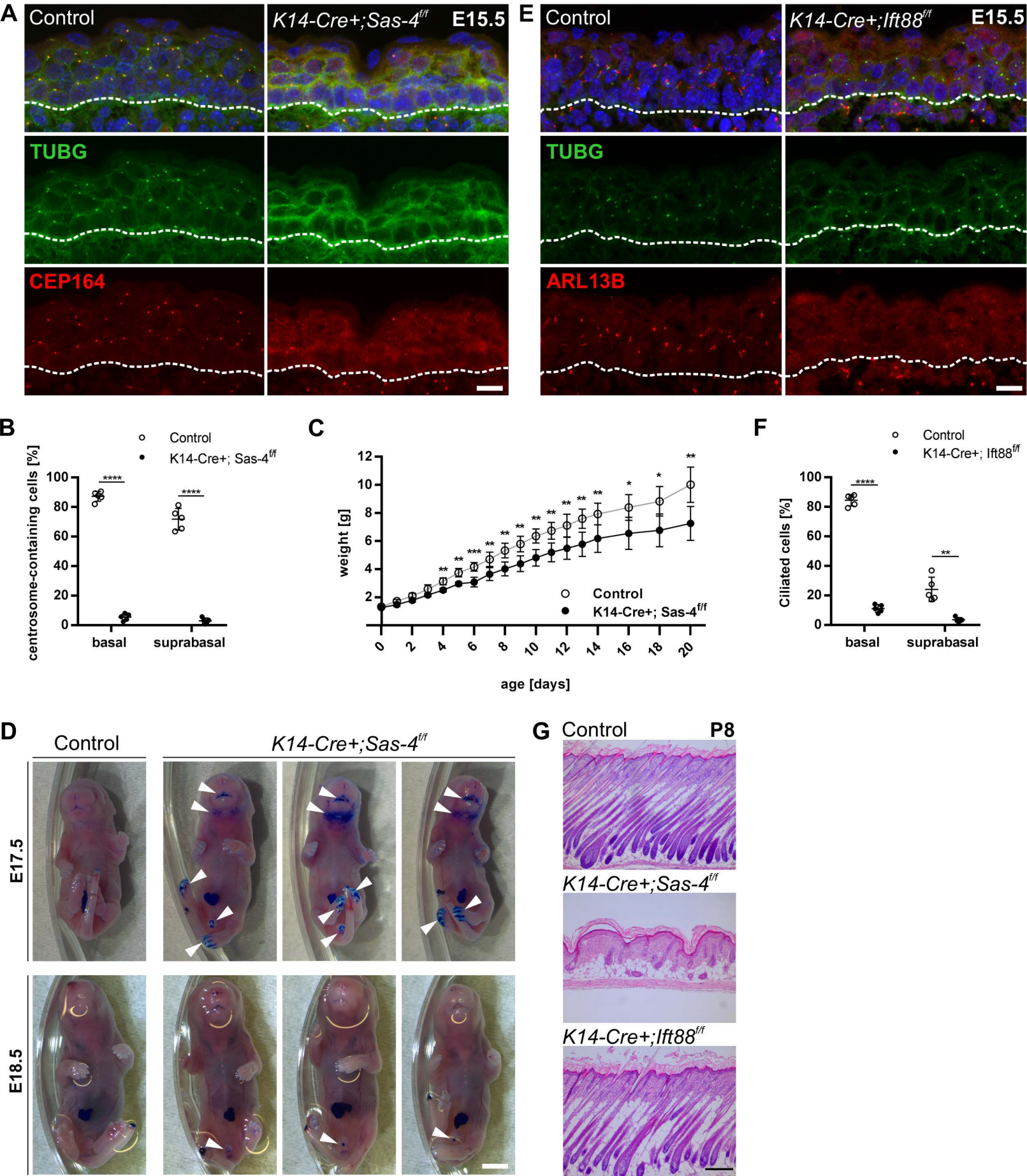
A
Control
K14-Cre+;Sas-4f/f
E15.5
TUBG
CEP164
E
Control
K14-Cre+;Ift88f/f
E15.5
TUBG
ARL13B
B
Control
K14-Cre+; Sas-4f/f
centrosome-containing cells [%]
****
****
basal
suprabasal
C
weight [g]
Control
K14-Cre+; Sas-4f/f
age [days]
F
Control
K14-Cre+; Ift88f/f
Ciliated cells [%]
****
**
basal
suprabasal
D
Control
K14-Cre+;Sas-4f/f
E17.5
E18.5
G
Control
P8
K14-Cre+;Sas-4f/f
K14-Cre+;Ift88f/f

Figure S2

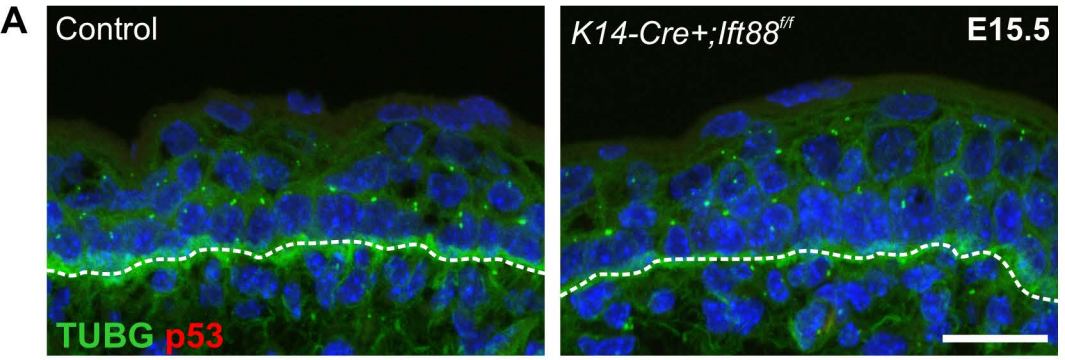

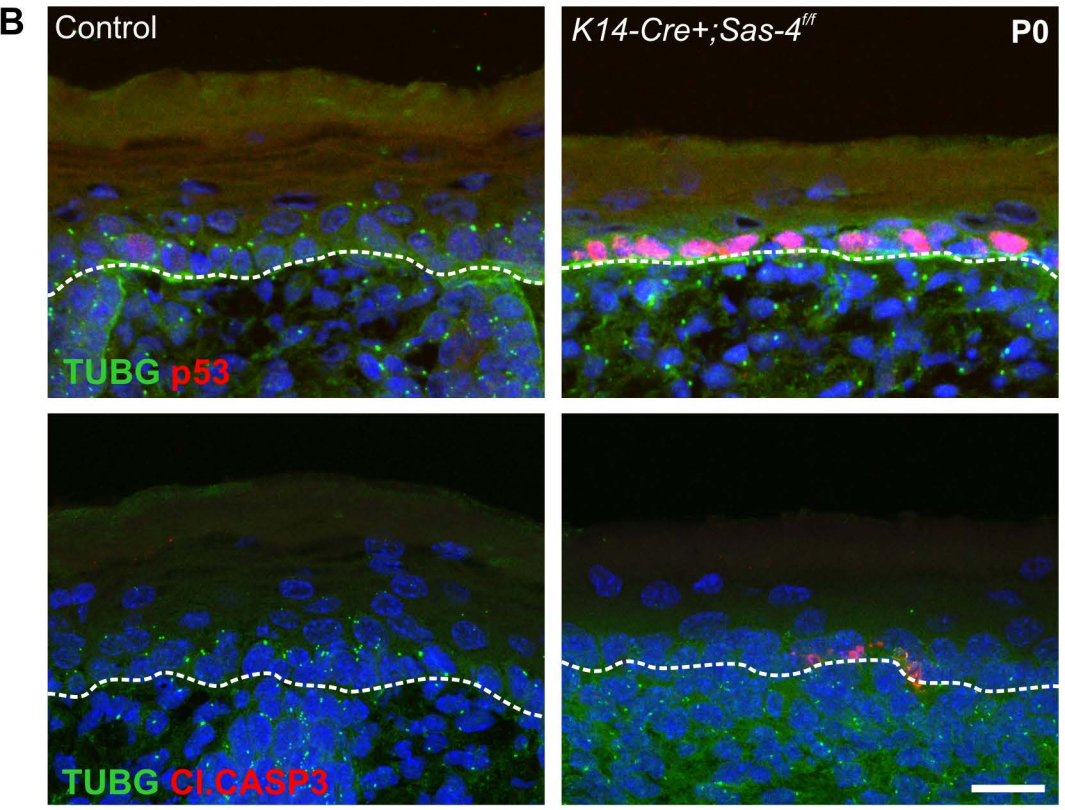

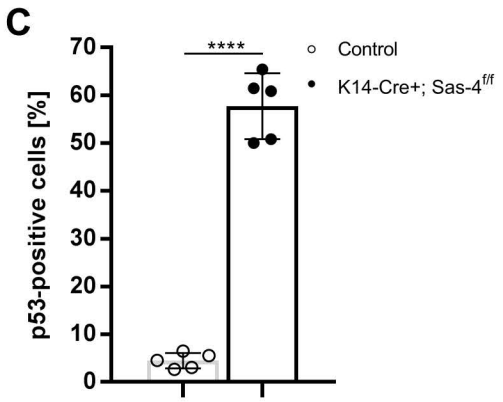

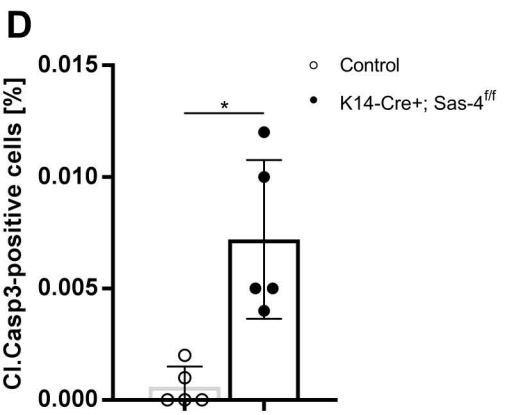

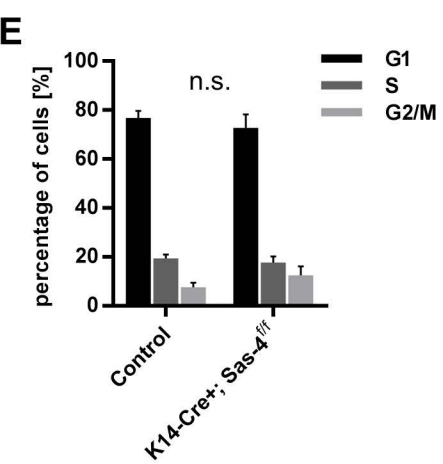

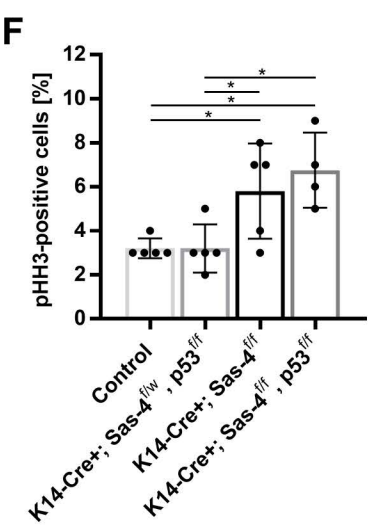

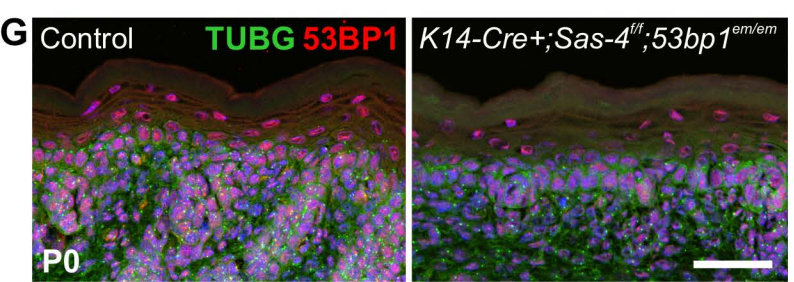

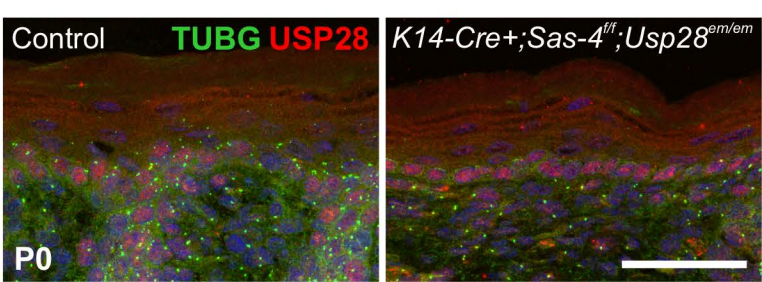

Figure S3

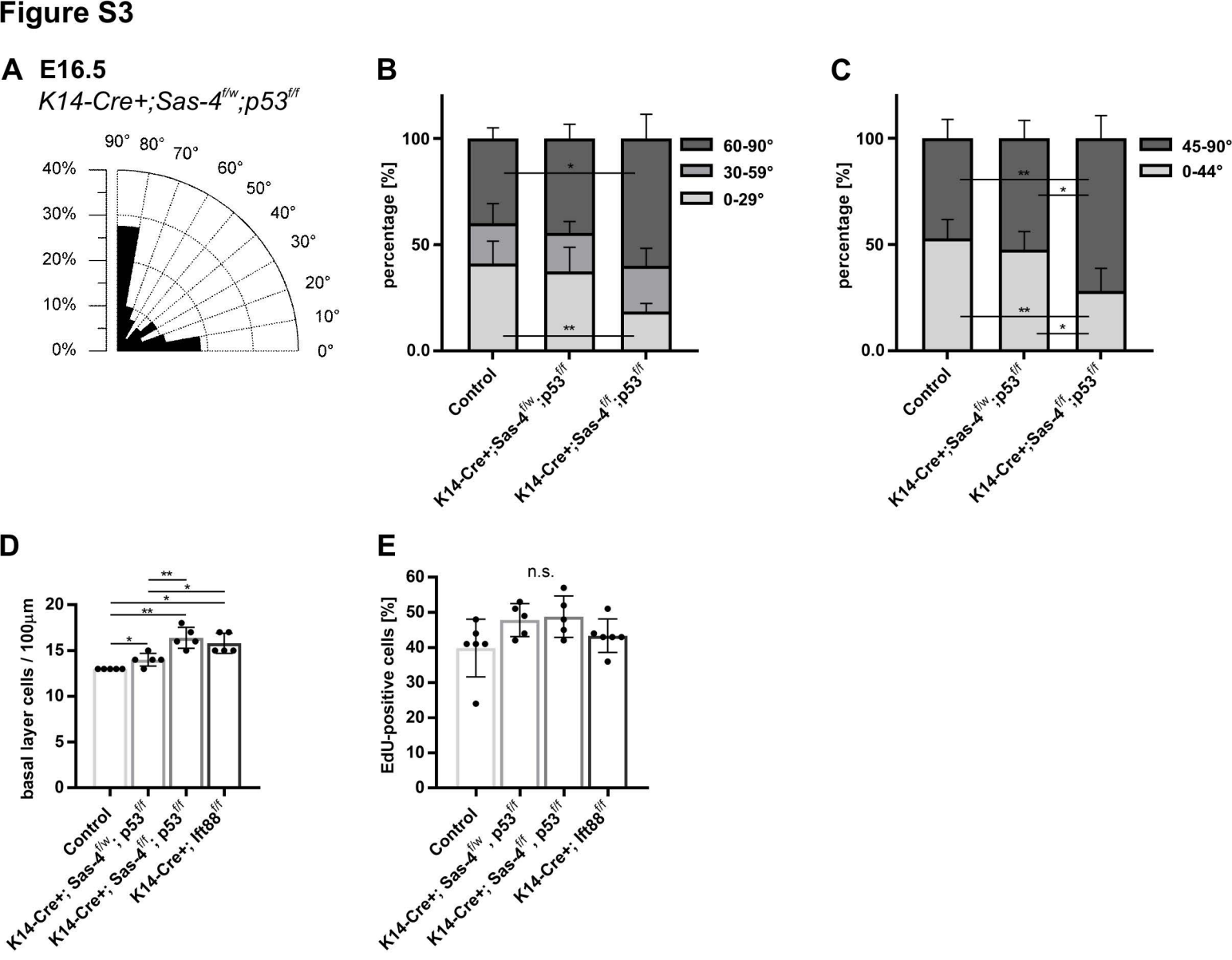
A
E16.5
K14-Cre+;Sas-4f/w;p53f/f
90° 80° 70° 60° 50° 40° 30° 20° 10° 0°
40% 30% 20% 10% 0%
B
percentage [%]
100
50
0.0
60-90°
30-59°
0-29°
*
**
Control
K14-Cre+;Sas-4f/w;p53f/f
K14-Cre+;Sas-4f/f;p53f/f
C
percentage [%]
100
50
0.0
45-90°
0-44°
**
*
**
*
Control
K14-Cre+;Sas-4f/w;p53f/f
K14-Cre+;Sas-4f/f;p53f/f
D
basal layer cells / 100µm
20
15
10
5
0
**
*
*
**
*
Control
K14-Cre+; Sas-4f/w; p53f/f
K14-Cre+; Sas-4f/f; p53f/f
K14-Cre+; Ift88f/f
E
EdU-positive cells [%]
60
50
40
30
20
10
0
n.s.
Control
K14-Cre+; Sas-4f/w; p53f/f
K14-Cre+; Sas-4f/f; p53f/f
K14-Cre+; Ift88f/f

Figure S4

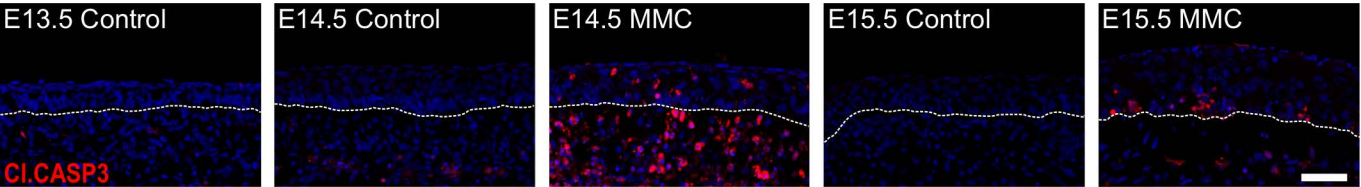
E13.5 Control
E14.5 Control
E14.5 MMC
E15.5 Control
E15.5 MMC
Cl.CASP3

Figure S5

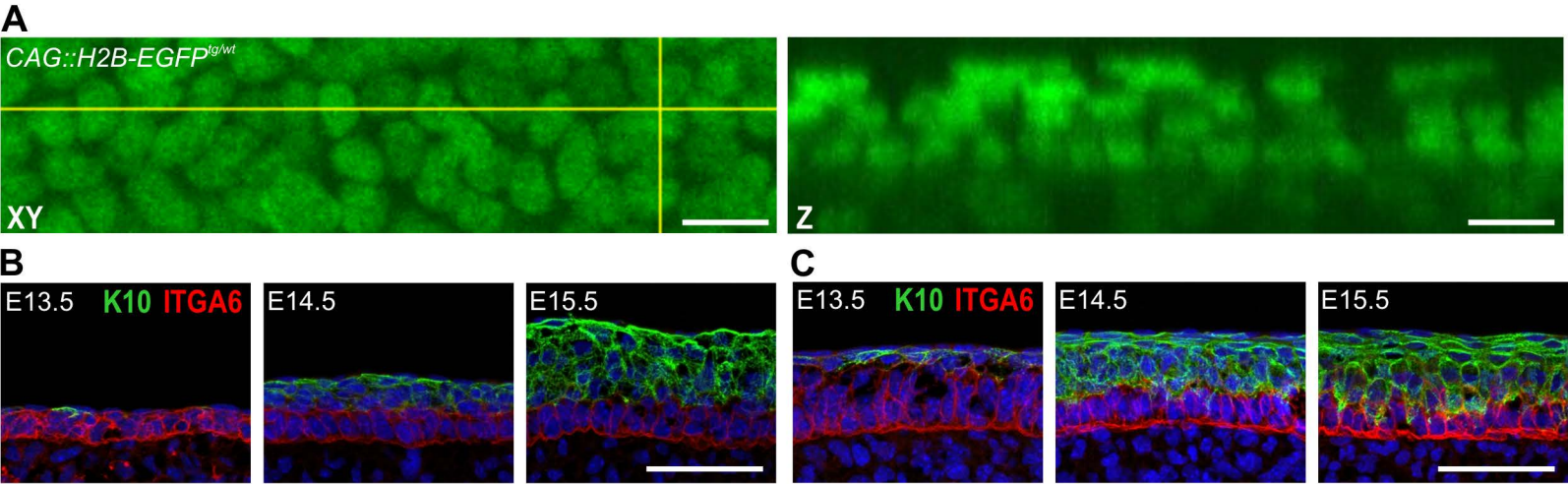
A
CAG::H2B-EGFPtg/wt
XY
Z
B
E13.5 K10 ITGA6
E14.5
E15.5
C
E13.5 K10 ITGA6
E14.5
E15.5

Figure S6

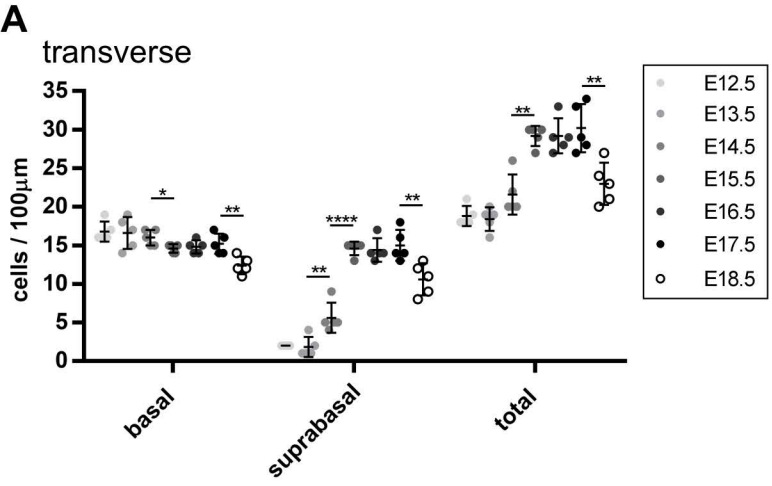
A
transverse
cells / 100µm
basal
suprabasal
total
E12.5
E13.5
E14.5
E15.5
E16.5
E17.5
E18.5

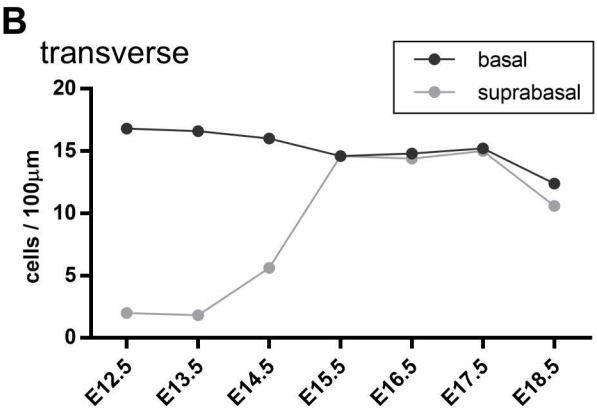
B
transverse
basal
suprabasal
cells / 100µm
E12.5
E13.5
E14.5
E15.5
E16.5
E17.5
E18.5

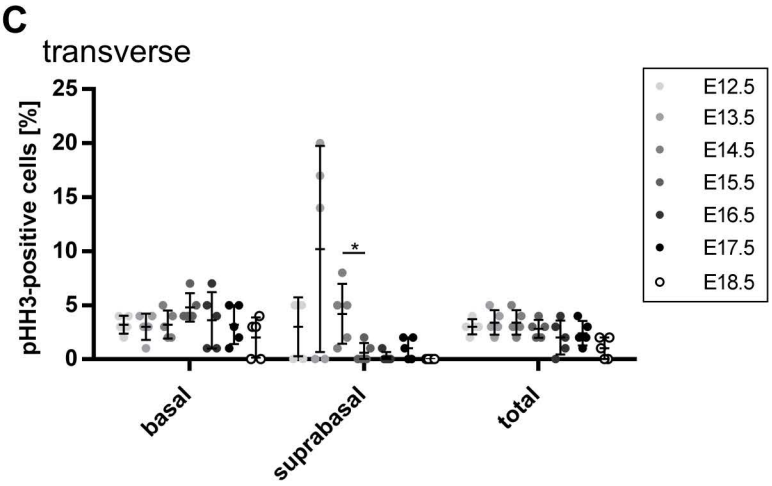
C
transverse
pHH3-positive cells [%]
basal
suprabasal
total
E12.5
E13.5
E14.5
E15.5
E16.5
E17.5
E18.5